AGU PUBLICATIONS

JGR

Journal of Geophysical Research: Atmospheres

RESEARCH ARTICLE
10.1002/2013JD021168

Key Points:
- Temperature changes by 10K with the spring and fall snow transitions
- A 10% decrease in days with snow cover increases winter temperatures by 1.4K
- With snow cover longwave cloud forcing dominates the diurnal cycle

Correspondence to:
A. K. Betts,
akbetts@aol.com

Citation:
Betts, A. K., R. Desjardins, D. Worth, S. Wang, and J. Li (2014), Coupling of winter climate transitions to snow and clouds over the Prairies, *J. Geophys. Res. Atmos.*, *119*, 1118–1139, doi:10.1002/2013JD021168.

Received 7 NOV 2013
Accepted 24 DEC 2013
Accepted article online 3 JAN 2014
Published online 4 FEB 2014

Coupling of winter climate transitions to snow and clouds over the Prairies

Alan K. Betts[1], Raymond Desjardins[2], Devon Worth[2], Shusen Wang[3], and Junhua Li[3]

[1]Atmospheric Research, Pittsford, Vermont, USA, [2]Agriculture and Agri-Food Canada, Ottawa, Ontario, Canada, [3]Natural Resources Canada, Ottawa, Ontario, Canada

Abstract Using data from 13 climate stations on the Canadian Prairies, together with opaque cloud cover and daily snow depth, to analyze the winter climate transitions with snow, we find that a snow cover acts as a fast climate switch. Surface temperature falls by about 10 K with fresh snowfall and rises by a similar amount with snowmelt, while the daily range of relative humidity falls to around 5–15% with snow cover. These are robust climate signals. For every 10% decrease in days with snow cover over the Canadian Prairies, the mean October to April climate is warmer by about 1.4 K. Stratifying by daily mean opaque cloud cover across snow transitions shows the rapid shift within 5 days from a diurnal cycle dominated by shortwave cloud forcing to one dominated by longwave cloud forcing. We calculate the change in the surface radiative budget with snow using surface albedo data from the Moderate Resolution Imaging Spectroradiometer and station longwave data. We find that with the fall-winter snow transitions, the surface radiative heating is reduced by 50 Wm^{-2}, with 69% coming from the reduced net shortwave flux, resulting from the increased surface albedo and a small increase in effective cloud albedo, and 31% from a reduced incoming longwave flux. This drop in surface radiative heating is sufficient to produce a drop in the surface radiometric skin temperature of 11 K. We find that in winter, the monthly mean diurnal climate is more closely coupled to the diurnal shortwave forcing than the mean diurnal climate.

1. Introduction

Northern latitudes are cold and have snow in winter. The traditional climatological view is that regions like the Canadian Prairies have snow because they are cold. Forecasters however have long noticed the large impact of snow cover on surface temperature and have estimated from case studies that snow cover reduces surface temperatures by about 5°C on both the short-term time scale and the monthly time scales [*Namias*, 1960, 1985; *Wagner*, 1973; *Dewey*, 1977]. *Groisman et al*. [1994] suggested that the retreat of the Northern Hemisphere's spring snow cover in the previous 20 years was linked to the observed increase of spring temperatures. *Mote* [2008] found that with deep snow, the surface maximum temperature was depressed 9.5°C, but the depression relative to the 850 hPa temperatures was reduced roughly in half to 4.6°C. The premise of this analysis was that the 850 hPa flow is uncoupled from the surface cooling with snow. However, *Viterbo and Betts* [1999] showed that the large regional errors in the albedo of snow propagate into large errors in the 850 hPa temperature within 5 days.

Models represent the coupled feedback, but quantitative answers are challenging because of the complexity of the land-boundary-layer-atmosphere coupling and the wide range of parameterizations in use. Early modeling studies estimated that the cooling of surface temperatures by snow cover could be as little as 1–2°C [*Cohen and Rind*, 1991] or as large as 10°C [*Walsh and Ross*, 1988]. At that time, there were large variations in the snow-climate feedback and in their cloud and longwave radiation interactions in general circulation models [*Cess et al*., 1991]. More recently, *Vavrus* [2007] showed that removing the hemispheric snow cover in a global climate model increases surface air temperatures over northern North America and Eurasia in winter by 8–10 K. However, *Bony et al*. [2006] showed that the relationship between surface albedo and temperature in spring in transient climate simulations in snow regions still varies by more than a factor of 3. They suggest that models should be constrained to reproduce the snow-albedo feedback in the present-day seasonal cycle, since *Hall and Qu* [2006] showed that the feedback simulated by these models for the present-day seasonal cycle is an excellent predictor of the snow-albedo feedback in the transient climate simulations. The development of improved representations of snow cover, surface albedo, and snow-albedo feedback in global models remains an important issue [*Lott and Graf*, 1993; *Roesch and Roeckner*, 2006; *Qu and Hall*, 2007].

Recently *Xu and Dirmeyer* [2013] developed a framework for evaluating the strength of snow-atmosphere coupling in global models.

Snow/ice albedo feedback is well known on global scales, but there has been rather little quantitative analysis of the role that shortwave feedback and longwave feedback play in the transitions with snow on local and regional scales, even though observers are aware that the large increase in the reflection of sunlight by snow cools the local climate [*Cohen*, 1994; *Betts*, 2011]. Our data analysis will provide a quantitative frame of reference for the Canadian Prairies, where the snow-albedo feedback is both large and uniform over an extensive region between roughly 49–53°N, 98–114°W. We will explore the coupling between snow cover, near-surface air temperature and humidity, and cloud cover using climate station data. We will show that over the Canadian Prairies, surface air temperature falls within days with fresh snowfall by about 10 K and rises by a similar amount with snowmelt. For the interannual variability for October to April on a regional scale, this fall of temperature increases to 13 to 15°C between cold seasons with no snow to those with 100% snow cover. The rapid fall-winter and winter-spring climate transitions that occur with snow cover suggest that the change in surface albedo with snow acts as a fast climate switch.

This paper will explore three of the coupled feedback that together drop the mean near-surface air temperature, T_m, by 10°C with snow cover. They are the large increase in surface albedo, a small increase in effective cloud albedo, and a drop in the downwelling longwave flux. There is a fourth contribution to the drop of air temperature: the upward ground heat flux is reduced [*Zhang et al*., 2008], because snow has much lower heat conductivity than soil. From an agricultural perspective, snow cover reduces the coupling between air and soil, and this limits soil freezing. Moreover, the protection of winter crops from frost damage depends on snow depth [*Thorsen et al*., 2010; *Trnka et al*., 2010], whereas the drop of air temperature is dependent more on snow albedo than on snow depth. *Dutra et al*. [2011] investigated the role of interannual snow cover variability in controlling the land-atmosphere coupling and its relation with soil and 2 m air temperature in 30 year climate simulations. They found that the interannual variability of snow cover and snow depth explains almost 60% of the winter interannual variability of 2 m T_m over north Eurasian and North American continents in regions that are predominantly snow covered. They also found a strong correlation between increasing snow depth, decreasing air temperature, and an increasing difference between soil and air temperature over the Midwestern U.S., between 35°N–45°N and 80–100°W.

This analysis will study the coupling of snow cover to the winter climate transitions and the fall, winter, and spring climate using the daily data sets for the period 1955–2006 for 13 Prairie climate stations, which were derived from hourly data by *Betts et al*. [2013a]. One unique aspect of these data is hourly estimates of opaque (or reflective) cloud cover, which can be calibrated on the daily time scale against incoming shortwave radiation to give the daily effective cloud albedo [*Betts et al*., 2013a]. From these data, we can estimate the longwave and shortwave cloud forcing (LWCF and SWCF, defined in section 7.1). We have sufficient high-quality, homogeneous data (over 600 station years) that we can derive the fully coupled response of the diurnal climate to both cloud and snow-albedo forcing over a range of time scales. *Betts et al*. [2013a] showed that the diurnal climate made rapid transitions in November and March between a winter state with snow and a warm season state without snow. These are the seasonal transitions into winter with the first snowfall and the first spring transition when the snowpack finally melts [*Betts*, 2011].

Specifically this paper will address five aspects of the winter climate at northern latitudes.

1. the winter climate transitions that occur with snowfall and snowmelt.
2. the coupling of the mean winter climate to snow cover.
3. the coupling of the diurnal cycle to cloud cover across snow transitions.
4. the change in the surface radiation budget with snow cover.
5. the shortwave forcing of the winter diurnal cycle.

In section 2, we discuss the data and our methodology for the snow transition composites and cloud stratification composites. Section 3 analyzes the climatology of the large winter and spring climate transitions that are coupled to snow cover. Section 4 shows the impact of snow cover on the mean winter climatology. Section 5 addresses how the coupling of the diurnal cycle to clouds shifts from SWCF control with no snow to LWCF control with snow. Section 6 shows the impact of snow cover on the surface shortwave albedo derived from the Moderate Resolution Imaging Spectroradiometer (MODIS) data. Section 7 discusses the change in the surface radiative budget across the fall snow transition. In section 8, we show the seasonal differences

Table 1. Climate Stations: Location and Elevation

Station Name	Station ID	Province	Latitude	Longitude	Elevation (m)
Red Deer[a]	3025480	Alberta	52.18	−113.62	905
Calgary[a]	3031093	Alberta	51.11	−114.02	1084
Lethbridge[b]	3033880	Alberta	49.63	−112.80	929
Medicine Hat	3034480	Alberta	50.02	−110.72	717
Grande Prairie[a]	3072920	Alberta	55.18	−118.89	669
Regina[a]	4016560	Saskatchewan	50.43	−104.67	578
Moose Jaw	4015320	Saskatchewan	50.33	−105.55	577
Estevan[a]	4012400	Saskatchewan	49.22	−102.97	581
Swift Current[b]	4028040	Saskatchewan	50.3	−107.68	817
Prince Albert[a]	4056240	Saskatchewan	53.22	−105.67	428
Saskatoon[a]	4057120	Saskatchewan	52.17	−106.72	504
Winnipeg[ab]	5023222	Manitoba	49.82	−97.23	239
The Pas[ab]	5052880	Manitoba	53.97	−101.1	270

[a]Complete data sets.
[b]Stations with downward shortwave radiation.

between the mean diurnal climate and the monthly mean diurnal climate following (A. Wang, and X. Zeng, Land surface air temperature diurnal range over high northern latitudes, *J. Clim.*, JCLI-D-13-00428, in revision, 2013) and find that the monthly mean diurnal climate is more consistent with the shortwave forcing. Section 9 presents our conclusions.

2. Data and Background

2.1. Climate Station Data

We analyzed the data from the 13 climate stations listed in Table 1: the stations are all at airports. These have hourly data, starting in 1953 for all stations, except Regina and Moose Jaw which start in 1954. However, the snow depth data, which is critical to this analysis, generally run from 1955 to 2006, and some station records finish earlier. The 10 southern stations from 49 to 52°N are in agricultural regions, and the three most northern stations (Prince Albert, The Pas, and Grand Prairie) are either in or close to the boreal forest.

2.2. Variables and Data Processing

The hourly climate variables include air pressure (p), dry bulb temperature (T), relative humidity (RH), wind speed and direction, total opaque cloud amount, and total cloud amount. Trained observers have followed the same cloud observation protocol for 60 years [*Manual of Surface Weather Observations*, 2013]. Opaque cloud is defined (in tenths) as cloud that obscures the Sun, Moon, and stars at night. Four stations, Lethbridge, Swift Current, The Pas, and Winnipeg, have downward shortwave radiation SW_{dn} for some of the period, and these were used to calibrate the daily mean total opaque cloud data in terms of SWCF [*Betts et al*., 2013a]. We generated a file of daily means of all variables, such as mean temperature and humidity, T_m, and RH_m and extracted and appended to each daily record the corresponding hourly data at the times of maximum and minimum temperature (T_x and T_n). We merged a file of daily total precipitation and daily snow depth. Since occasional hourly data were missing, we kept a count of the number of measurement hours, MeasHr, of valid data in the daily mean. In our results, here we have filtered out all days for which MeasHr < 20. However, with almost no missing hours of data in the first four decades, there are very few missing analysis days, except for Swift Current, where nighttime data are missing from June 1980 to May 1986, and Moose Jaw, where nighttime measurements ceased after 1997.

Our analysis framework is based on the concept of the land-surface diurnal cycle climate, introduced by *Betts and Ball* [1995, 1998] for a grassland study, used by *Betts* [2004] to discuss hydrometeorology in global models, and discussed in detail by *Betts et al.* [2013a]. For individual days, the diurnal cycle is a combination of local processes and synoptic scale advection. However, if sufficient data are composited (see sections 2.3 and 2.4), the climatology representative of transitions with snow or changing cloud cover emerges from the synoptic variability.

We define the diurnal temperature range between maximum temperature, T_x, and minimum temperature, T_n, as

$$DTR = T_x - T_n \quad (1)$$

We also define the difference of relative humidity, RH, between T_n and T_x, as

$$\Delta RH = RH{:}T_n - RH{:}T_x \approx RH_x - RH_n \quad (2)$$

where RH_x and RH_n are the maximum and minimum RH. This approximation is excellent in the warm season, when surface heating couples with a convective boundary layer (BL). Then typically RH reaches a maximum near sunrise at T_n and a minimum at the time of the afternoon T_x [*Betts et al*., 2013a]. However, in winter, especially with snow cover, the diurnal solar forcing is greatly reduced compared to summer, while daily advective changes are larger than in summer. As a result, both DTR and ΔRH become dominated by the daily advective changes. This has a large impact on the climatology of DTR, as suggested in a recent paper by (Wang and Zeng, in revision, 2013). ΔRH is itself small at cold temperatures in winter. We address the conceptual impacts on the climatology of both DTR and ΔRH in section 8. We also derived from *p*, *T*, and RH the lifting condensation level (LCL), mixing ratio (*Q*), and the pressure height to the LCL, P_{LCL}.

2.3. Snow Transition Composite Methodology

We constructed a climatology of snow dates for each station by identifying the dates of the first lasting snowfall in the autumn and the date when the winter snowpack disappeared in spring. We then generated mean transitions by compositing 15 days before and after these surface snow events. Simple "ideal" transitions are where the ground is snow free, then heavy snow falls, and the ground stays snow covered until the snowpack melts in spring, followed again by snow-free ground. This happens in many years for the central Prairie stations, especially the more northern ones. In the fall, there are years, especially in southwestern Alberta, where the winter climate is warmer, when snow falls, and then melts. For these cases, we looked for snow transitions where the ground was snow free for a week ahead and snow covered the week after. Nature always presents some more complex situations: for example, when a little snow falls and then melts a few days ahead of a major snowfall, or there is a brief snowfall in spring shortly after the melt of the winter snowpack. For a few years, we had to make a choice between accepting a more complex transition or simply not including a case for that year and season. However, for most stations, we have 40–50 years of data, and excluding a few years does not impact the climatology. We chose only one transition in the fall and spring for the main analysis. For our analysis of the long-wave transition in section 7.3, where we had only a single station, we looked for all the possible snow transitions in the fall to increase the sample size for analysis.

The variability across snow events is of course large, as it depends on the structure of different weather systems embedded in a highly variable large-scale flow. Given sufficient data (we have over 600 station years), compositing about a distinct physical event like snowfall, which has a large impact on the surface energy balance, reduces by averaging the highly variable advection and extracts a climatology of the transition. We will illustrate this with several approaches (see section 3). We first generated composite transitions for each station and then merged these in groups to give means and show the variability between stations.

2.4. Cloud Stratification Composites

The second analysis tool we shall use is to further stratify composite snow transitions by daily mean opaque cloud cover, following *Betts et al*. [2013a, 2013b]. One remarkable feature of this Canadian data set is the estimation by trained observers of hourly opaque cloud cover (in tenths), for nearly six decades, with almost no missing observations. The excellent quality of these data is such that the daily mean opaque cloud cover can be calibrated against incoming solar radiation and longwave fluxes [*Betts et al*., 2013a]. This will enable us to show how the changing SWCF and LWCF are linked to the changing surface response across snow transitions.

3. Winter and Spring Snow Transitions

The winter and spring snow transitions are a central feature of high-latitude seasonal climate. *Betts et al*. [2013a] showed that the diurnal climate across the Prairies made rapid transitions in November and March between two distinct states: a winter state with snow cover and a warm season state without snow. They suggested that the diurnal cycle is coupled to the winter climate transition [*Betts*, 2011], when the first lasting snow cover has a large local climate impact. They showed a 1955–1993 composite of the fall-winter transitions for Regina, which on average occurs in mid-November. They noted that over 3 days across the snow event, T_x falls about 8°C, T_n by about 5°C, while ΔRH falls from about 20% to its typical winter value below 5%. This was the impetus for the more detailed analysis we present here.

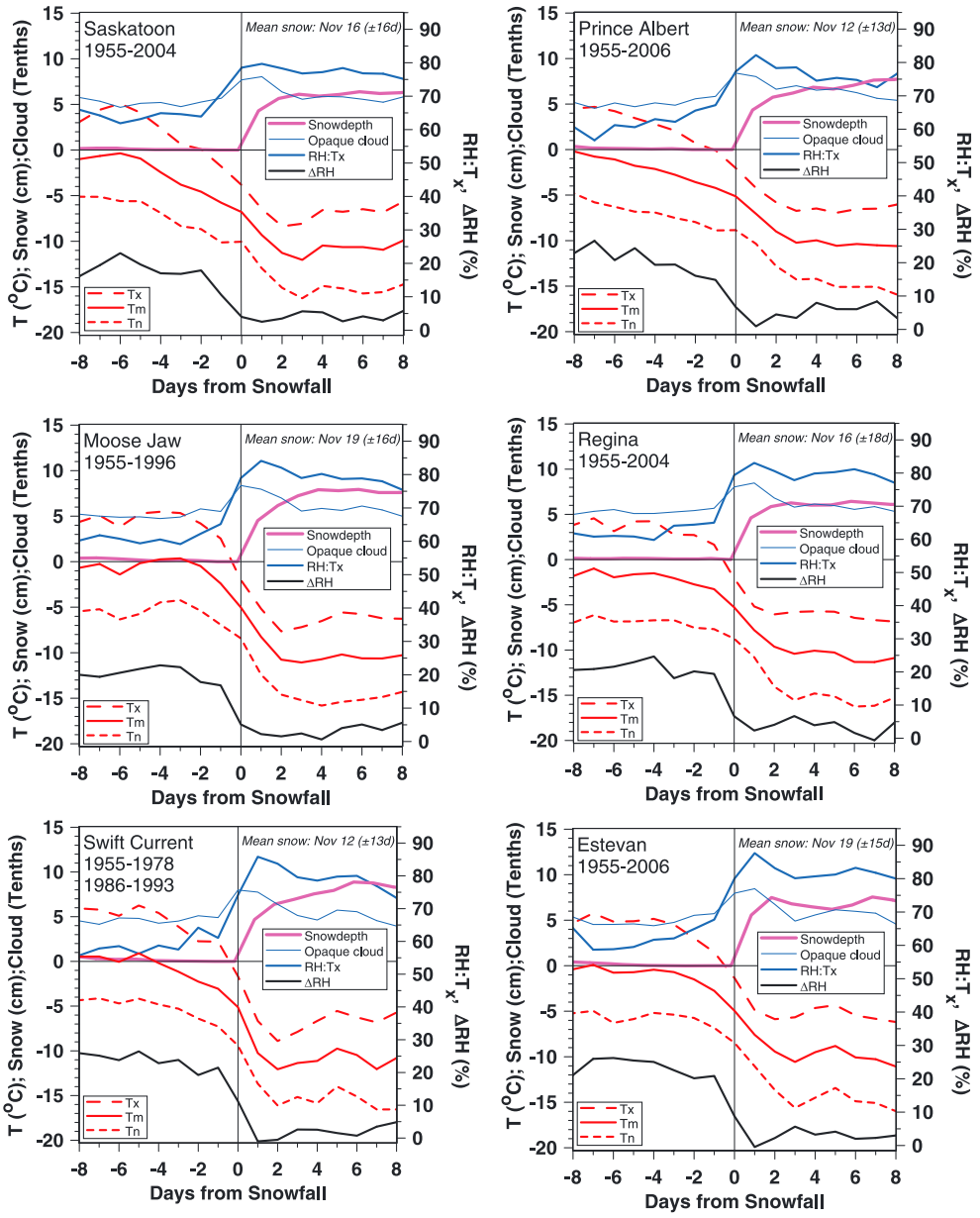

Figure 1. Climatology across the fall-winter snow transitions, marked as day 0, for six climate stations in Saskatchewan.

3.1. Fall-Winter Transitions

Figure 1 shows the climatology across the fall-winter snow transitions for six climate stations in Saskatchewan. All stations have more than 30 years of data and four have 50 years. The patterns are very similar. Average snow dates are mid-November with a station standard deviation of about ±15 days. Opaque cloud cover rises from about 5/10s before snow to a peak ≈8/10s at days 0 and 1 and then falling to about 6/10s. Five days before the snow event, $T_m \approx -1$°C, while $T_x \approx +4$°C. T_x falls below freezing just ahead of the snowfall. Across the transition, temperatures fall by −9 to −10°C, with T_x falling ahead of T_n. The diurnal range ΔRH falls from 22% to its typical low winter value of about 4%, as RH:T_x increases from 61 to 79%, while RH:T_n is unchanged at 83% (not shown).

The transitions in Figure 1 are very similar across this group of six stations in Saskatchewan, so we then generated a mean transition with the standard deviation across the six station climatologies. This is shown in

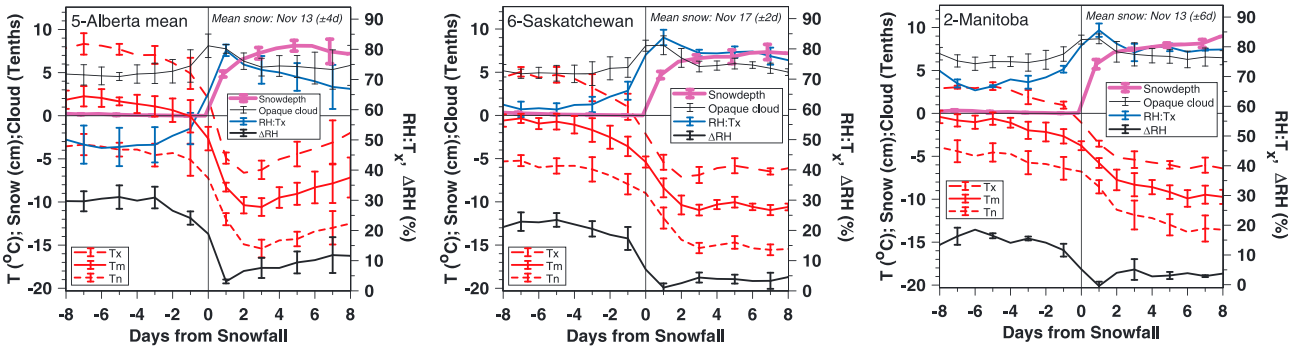

Figure 2. Mean fall-winter transitions with snow by province.

Figure 2 (middle), together with the corresponding panels for the five stations in Alberta and the two stations in Manitoba.

We see broad similarities and some differences from west to east across the Prairies. T_x, T_m, T_n, and ΔRH all fall across the snow boundary, and RH:T_x rises, peaking with the snowfall close to saturation over ice (not shown). Opaque cloud cover peaks for days 0 and 1 near 8/10s, and typically cloud cover is higher after the snow transitions than before. Table 2 summarizes the mean change in T_x, T_m, T_n, RH, cloud, and other variables across the snow transitions for the three provincial composites. We averaged the variables for the 5 day ranges from −7 to −3 days ahead and from 3 to 7 days after snow and found the mean difference and standard deviation.

The fall of temperature and humidity variables varies little within each group. There appears to be a decrease from west to east, but we have only two stations in Manitoba, and one of them, The Pas, is within the boreal forest. Manitoba may also be influenced by a large number of lakes. There could be differences in advection as the climate of Alberta is more influenced by maritime flows from the Pacific, than are the central and eastern parts of the Prairies.

3.2. Fall Snow Transition Compared With Climatology

Figure 3 embeds the mean composite transition, 15 days before snow event and 15 days after (solid lines), within the corresponding mean climatology (dotted lines) for October to December for the six Saskatchewan climate stations. Figure 3 (left) contrasts the smooth climatological increase of snow and the fall of T_m and ΔRH, found by averaging by day of year, with the sharp transition that occurs when we composite about the snow events, with a mean date of 17 November. Figure 3 (right) corresponds for mixing ratio (Q) and the pressure height of the LCL (P_{LCL}) at the time of T_x. Note the sharp fall in P_{LCL} and Q across the snow transition. In essence, the 30 day transition in the climatology occurs within a few days with major snow events, whose date varies by ±15 days.

Table 2. Change Across the Fall Snow Transitions for the Three Provincial Composites

	5-Alberta			6-Saskatchewan			2-Manitoba		
Variable	−7 to −3 d	3 to 7 d	Difference	−7 to −3 d	3 to 7 d	Difference	−7 to −3 d	3 to 7 d	Difference
T_m (°C)	1.7 ± 0.9	−9.1 ± 1.5	−10.7 ± 0.8	−1.0 ± 0.7	−10.6 ± 0.4	−9.6 ± 0.8	−1.1 ± 0.8	−9.1 ± 1.0	−8.0 ± 0.2
T_x (°C)	7.7 ± 0.9	−4.5 ± 1.7	−12.2 ± 1.0	4.3 ± 0.8	−6.3 ± 0.6	−10.6 ± 0.7	2.8 ± 0.4	−5.9 ± 0.7	−8.7 ± 0.3
T_n (°C)	−3.9 ± 1.0	−14.1 ± 1.1	−10.2 ± 0.9	−5.8 ± 0.8	−15.2 ± 0.4	−9.4 ± 0.8	−4.9 ± 1.2	−12.9 ± 1.4	−8.0 ± 0.2
RH_m (%)	65.5 ± 5.1	76.4 ± 3.4	10.9 ± 2.0	74.4 ± 1.3	81.1 ± 1.6	6.7 ± 1.8	76.8 ± 0.0	81.3 ± 0.7	4.5 ± 0.6
RH:T_x(%)	48.0 ± 5.8	70.7 ± 5.4	22.7 ± 1.9	60.7 ± 1.8	78.6 ± 2.0	17.9 ± 3.0	67.4 ± 0.0	79.1 ± 1.6	11.7 ± 1.6
ΔRH (%)	30.4 ± 2.5	9.3 ± 4.4	−21.1 ± 2.7	22.3 ± 2.0	3.8 ± 1.3	−18.5 ± 2.7	16.2 ± 0.4	3.5 ± 1.5	−12.6 ± 1.9
Q (g/kg)	3.4 ± 0.3	2.3 ± 0.2	−1.1 ± 0.3	3.4 ± 0.1	2.2 ± 0.1	−1.2 ± 0.1	3.3 ± 0.1	2.2 ± 0.0	−1.1 ± 0.1
P_{LCL} (hPa)	145 ± 18	70 ± 14	−75 ± 8	103 ± 5	47 ± 5	−56 ± 8	84 ± 0.4	48 ± 4	−36 ± 5
Cloud (Tenths)	4.7 ± 0.3	5.6 ± 0.5	0.9 ± 0.3	4.9 ± 0.3	5.8 ± 0.4	0.9 ± 0.4	6.0 ± 0.2	6.6 ± 0.5	0.6 ± 0.3
Snow depth (cm)	0.1 ± 0.0	7.8 ± 0.9	7.6 ± 0.9	0.2 ± 0.1	6.9 ± 0.7	6.8 ± 0.7	0.2 ± 0.0	7.9 ± 0.3	7.7 ± 0.4

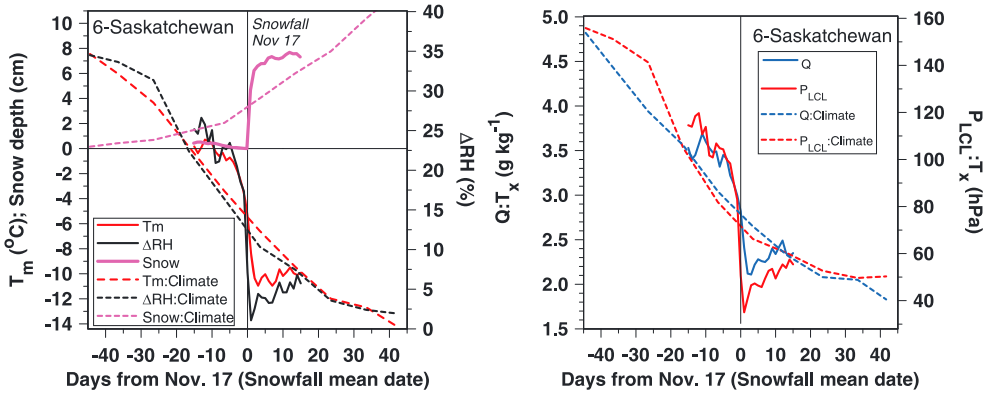

Figure 3. Comparison of composite fall snow transitions with mean climatology for Saskatchewan.

3.3. Winter-Spring Transitions

Figure 4 shows three groupings of the transitions with snowmelt in spring. Three southwestern stations in Alberta (Calgary, Lethbridge, and Medicine Hat) are the group shown in Figure 4 (left). Here snowmelt is frequent during the winter, and the climatology of the final snowmelt occurs the earliest. The snowpack a week before melt is only 8 cm deep, the transition to no snow lasts about 5 days, and the temperature increases about 11°C across the transition. Figure 4 (middle) presents seven Prairie stations (Red Deer, Estevan, Moose Jaw, Regina, Saskatoon, Swift Current, and Winnipeg). The initial snowpack is a little deeper (14 cm), melt lasts longer (10–14 days), ending around 26 March, and temperature increases about 10°C across the transition. Figure 4 (right) is for the three most northern stations (Grand Prairie, Prince Albert, and The Pas), where the snowpack is deepest and final snowmelt comes latest (11 April). Here snowmelt lasts about 25 days, with a gradual rise of temperature of 10°C over this whole period.

Table 3 summarizes the mean change in T_x, T_m, T_n, RH, cloud, and other variables across the snowmelt transitions for these three composites. We averaged the variables for the 5 day range from 3 to 7 days after snowmelt. The longer the snowpack took to melt, the further back we took the average before melt. We used −7 to −3 days ahead in southwest Alberta, −14 to −10 days ahead for the seven Prairie stations, and back to −25 to −21 days ahead for the three northern stations. In Table 3, we reversed the sign of the differences to facilitate direct comparison with Table 2. The differences with snow on the ground are very similar: temperatures are about 10°C cooler, ΔRH is about 15–20% lower, and opaque cloud cover is a little higher (although the difference with snow is smaller with the winter-spring than the fall-winter transitions). If we average across all six composites in Tables 2 and 3, we see that snow cover produces a fall in T_m, T_x, and T_n of −9.9 ± 1.0, −10.6 ± 1.1, and −10.0 ± 1.2°C.

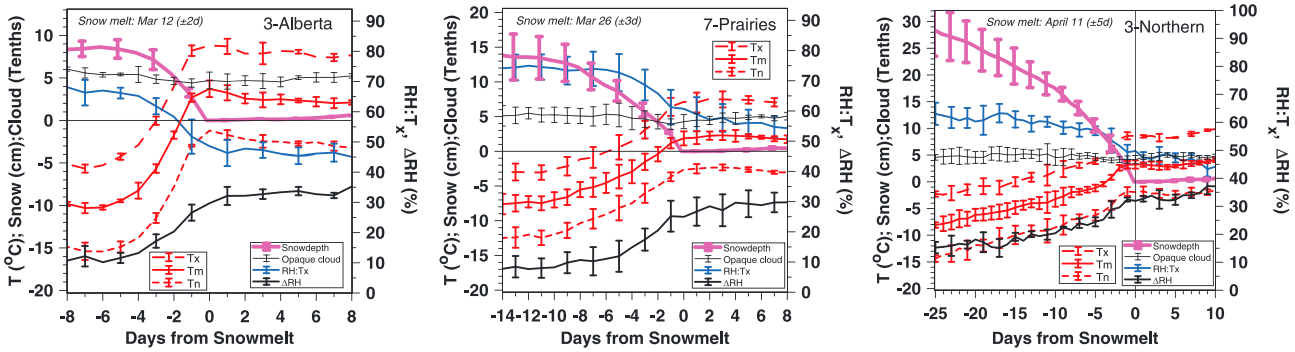

Figure 4. Mean winter-spring transitions with snow for three groupings of stations.

Table 3. Change Across the Spring Snowmelt for Three Composites

	3-Alberta			7-Prairies			3-Northern		
Variable	−7 to −3 d	3 to 7 d	Difference	−14 to −10 d	3 to 7 d	Difference	−25 to −21 d	3 to 7 d	Difference
T_m (°C)	−8.8 ± 0.4	2.3 ± 0.5	−11.1 ± 0.9	−7.4 ± 0.4	2.1 ± 0.4	−9.5 ± 0.9	−7.5 ± 1.2	3.1 ± 0.5	−10.5 ± 0.7
T_x (°C)	−3.6 ± 0.4	7.8 ± 0.5	−11.4 ± 0.9	−3.0 ± 0.6	7.3 ± 0.6	−10.3 ± 0.9	−2.1 ± 1.1	8.6 ± 0.5	−10.6 ± 0.7
T_n (°C)	−14.2 ± 0.6	−2.7 ± 0.4	−11.5 ± 1.1	−12.3 ± 0.3	−2.6 ± 0.3	−9.6 ± 1.2	−13.4 ± 1.5	−2.2 ± 0.8	−11.1 ± 0.8
RH_m (%)	73.4 ± 1.5	64.5 ± 2.4	9.0 ± 2.2	79.9 ± 2.7	73.0 ± 2.6	6.9 ± 2.2	71.4 ± 2.9	65.5 ± 1.2	5.9 ± 2.8
RH:T_x(%)	65.3 ± 2.5	46.3 ± 2.5	19.0 ± 2.8	74.5 ± 4.2	56.1 ± 3.7	18.4 ± 4.1	61.9 ± 3.7	47.5 ± 1.9	14.4 ± 5.1
ΔRH (%)	12.9 ± 2.2	33.0 ± 1.4	−20.1 ± 2.9	8.0 ± 3.2	28.9 ± 3.7	−20.9 ± 3.5	15.9 ± 2.2	33.0 ± 2.2	−17.1 ± 4.2
Q (g/kg)	2.4 ± 0.1	3.3 ± 0.2	−0.9 ± 0.1	2.6 ± 0.2	3.8 ± 0.1	−1.1 ± 0.2	2.3 ± 0.2	3.4 ± 0.0	−1.13 ± 0.2
P_{LCL} (hPa)	80 ± 7	148 ± 8	−68 ± 10	60 ± 15	124 ± 14	−64 ± 13	96 ± 13	152 ± 4	−56 ± 16
Cloud(Tenths)	5.3 ± 0.3	4.9 ± 0.1	0.5 ± 0.3	5.3 ± 0.4	4.9 ± 0.3	0.4 ± 0.5	4.7 ± 0.5	4.8 ± 0.3	0.1 ± 0.5
Snow depth(cm)	8.1 ± 0.9	0.2 ± 0.0	7.9 ± 1.0	13.5 ± 3.1	0.3 ± 0.1	13.3 ± 0.1	27.3 ± 4.4	0.22 ± 0.2	27.0 ± 4.2

4. Impact of Snow Cover on Mean Climatology

4.1. Fall and Spring Climatology

In the previous section, we selected single transitions in fall and spring to construct a homogeneous climatology of the large climate transitions across snow boundaries that often occur within days. One simple and important consequence is that the mean climatology depends on all the transitions that occur in the cold season and explicitly depends directly on the fraction of days with snow cover. For the transition periods, October, November, and December, and March and April, we computed the means of T_m, ΔRH, and FDS, the fraction of days in each period that are snow covered, for each of the five Alberta stations (about 240 station years of data) and the six Saskatchewan stations (about 270 station years of data). We then removed the bias between the station means to give bias-corrected values, T_{mb}, RH_{mb}, FDS_b, which are plotted in Figure 5.

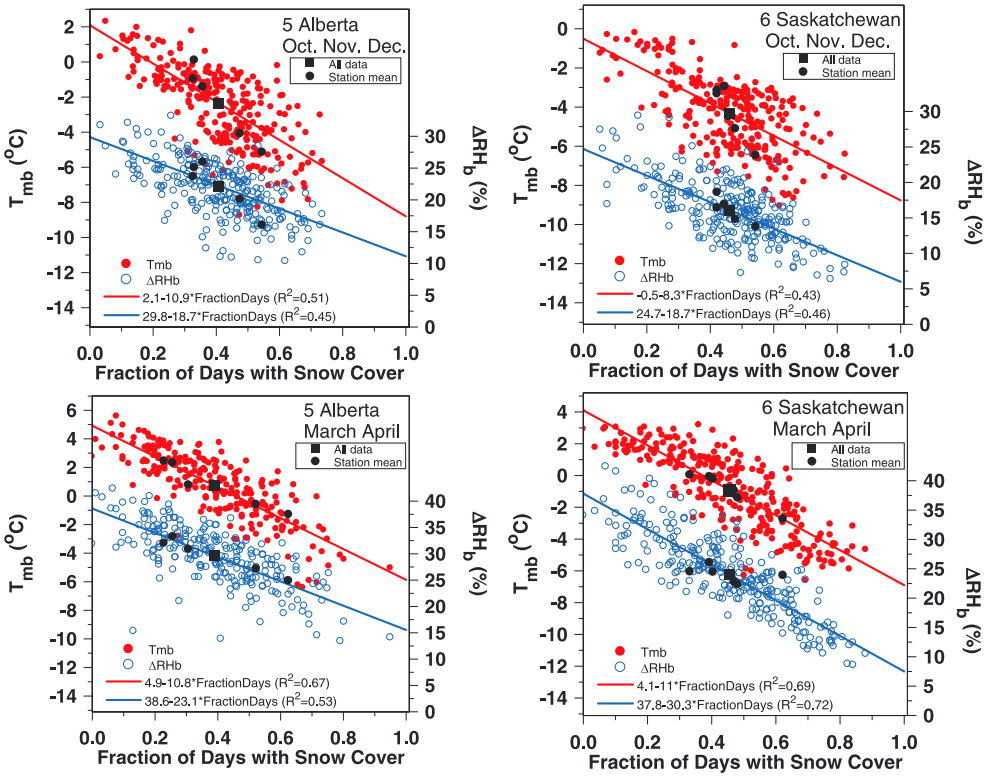

Figure 5. T_{mb} and ΔRH_b plotted against fraction of days with snow cover.

Table 4. Linear Regression Fits (Equation (3))

	A (°C)	B (°C)	R^2	C (%)	D (%)	R^2	E (%)	G	H	R^2
5AB:OND (October-November-December)	2.1 ± 1.5	−10.9 ± 0.7	0.51	29.8 ± 3.0	−18.7 ± 1.3	0.45	11.1	4.6 ± 0.7	1.2 ± 0.2	0.13
6SK:OND	−0.5 ± 1.4	−8.3 ± 0.6	0.43	24.7 ± 3.0	−18.7 ± 1.3	0.52	6.0	4.7 ± 0.5	0.8 ± 0.2	0.05
5AB:MA (March and April)	4.9 ± 1.3	−10.8 ± 0.5	0.67	38.6 ± 3.8	−23.1 ± 1.4	0.53	15.5	4.7 ± 0.5	1.3 ± 0.2	0.17
6SK:MA	4.1 ± 1.4	−11.0 ± 0.4	0.69	37.8 ± 3.5	−30.3 ± 1.1	0.72	7.5	4.7 ± 0.5	1.1 ± 0.2	0.12
Mean		−10.2 ± 1.1		32.7 ± 5.7			10.0 ± 3.6		1.1 ± 0.2	

The plotted points are all perturbations from the solid black square, which is the mean of all the station data. The solid black circles are the individual station means: their spread has been removed by the bias correction. The stations that are coldest with the most snow are the most northern ones: Grand Prairie in Alberta and Prince Albert in Saskatchewan. If we do not remove the interstation biases, we get higher regression line slopes in the fall (but not in the spring), as shown by the steeper slope of the station means in the fall compared to the regression line plotted for the bias-corrected data.

Table 4 gives the coefficients of the linear regression line fits with the form

$$T_{mb} : \text{fit} = A + B * FDS_b \quad (3a)$$

$$\Delta RH_b : \text{fit} = C + D * FDS_b \quad (3b)$$

$$\text{OpaqueCloud}_b : \text{fit} = G + H * FDS_b \quad (3c)$$

The interannual variability is large and the R^2 coefficients for T_{mb}:fit and ΔRH_b:fit varies between 43 and 72%; they are generally larger for the March–April snowmelt period in spring than for the October-November-December transitions into winter with snow. The column E in Table 4 is the value of ΔRH for $FDS_b = 1$, when all days have snow cover. The opaque cloud fit coefficient H shows a small increase with increasing snow cover, but note that the R^2 coefficients are small.

We see that the transition from 0 to 1 in the fraction of snow days drops the mean temperature by −10.2 ± 1.1°C, while the fall of ΔRH_b shows the transition between warm and cold season states. These numbers correspond closely to the mean transition across snow boundaries we see in Tables 2 and 3 and Figures 3 and 4. The transition from 0 to 1 in the fraction of snow days increases the opaque cloud cover by 11 ± 2%, larger than the 9% and 4.5% increases seen in Tables 2 and 3.

We looked separately at the three most northern stations (Grand Prairie, Prince Albert, and The Pas). For the March and April snowmelt period, the temperature fit has a slope of B = −10.7 ± 0.7, and the corresponding October, November, and December fit is B = −10.7 ± 1.0 (not shown). These values are similar to those in Tables 3 and 4. This is somewhat surprising since these stations have the most forest within 50 km [*Betts et al.*, 2013b], and the forest has a much lower albedo with snow than grassland (see Figure 10) [*Betts and Ball*, 1997]. Even the single station within the boreal forest, The Pas, has similar mean values of B = −10.2 ± 2.5 in the fall and −10.7 ± 1.3 in the spring (not shown). We considered the possibility that the airport data over grass might not be representative of the boreal forest, by comparing the 1994–1996 data from the Boreal Ecosystem-Atmosphere Study (BOREAS) at a forest tower only 3 km from the airport climate station at The Pas. The correlation between the two data sets for T_m is extremely high ($R^2 = 0.99$), and the systematic differences are very small. With snow cover, the airport data over grass have a daily mean temperature that is +0.3°C warmer than the tower data at 2 m above the forest floor and −0.5°C cooler than the tower data a few meters above the forest canopy.

Although the increase of surface albedo with snow is larger over the Prairies than the boreal forest, we will see in section 7 that the radiative changes with snow involve other important terms. The fall of LW_{dn} with snow cover contributes about 31% of the surface cooling, while the increase of cloud cover introduces partly canceling changes in the SWCF and LWCF. In addition, there may be a regional influence of the cooling of the Prairies with snow cover that extends into the boreal forest.

4.2. Winter Climatology

We then looked at the impact of snow cover on the mean climatology for the 7 month "cold season" period from October to April, when snow may occur on the Canadian Prairies. This merges January and February with the two transitions shown in Figure 5. Figure 6 (top row) is similar to those in Figure 5, with the removal

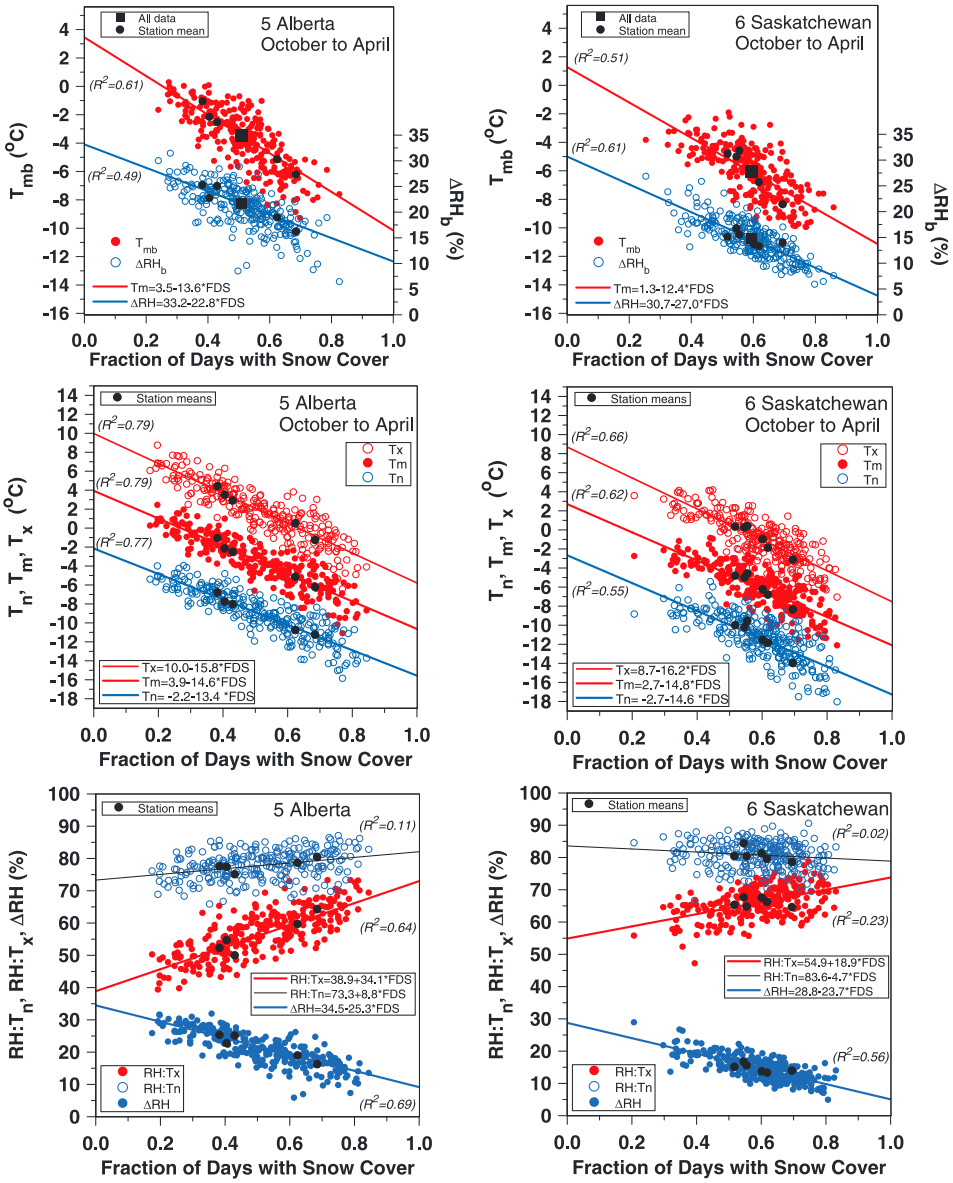

Figure 6. T_{mb} and ΔRH_b plotted against fraction of days with (top row) snow cover, (middle row) T_x, T_m, and T_n, and (bottom row) RH:T_n, RH:T_x, and ΔRH against fraction of days with snow cover.

of the bias between station means. However, the mean bias between stations has a very similar correlation: snow cover increases with the temperature gradient from west to east and south to north across the Prairies. So from a regional perspective, we show in Figure 5 (bottom row) the direct plot of T_x, T_m, T_n, and RH:T_n, RH:T_x, and ΔRH against fraction of days with snow cover.

Table 5 shows the linear regression fits to the data in Figure 6. For the five Alberta stations, where winter snow cover is usually transient except for Grande Prairie, the linear regression explains as much as 77–79% of the variance (Figure 6, middle row) in the 7 month mean climate for T_x, T_m, and T_n. For the six Saskatchewan stations, the variance explained is a little less. The temperature slopes with FDS are similar for both Alberta and Saskatchewan, increasing from -13.0 ± 0.8 for T_m, with the interstation biases removed, to -14.0 ± 0.7, -14.7 ± 0.6, and -16.0 ± 0.6 for T_n, T_m, and T_x, for the regional data, without removing interstation biases. These slopes are larger than in Tables 2, 3, and 4, suggesting that there is a further regional feedback with snow cover that cools the Prairies on this longer 7 month time scale [*Namias* 1985]. Note that the T_x cools more than T_n in Table 5.

Table 5. Winter Linear Regression Fits

	A (°C)	B (°C)	R^2	C (%)	D (%)	R^2	E (%)	G	H	R^2
5AB:FDS_b	3.4 ± 1.2	−13.6 ± 0.7	0.61	33.2 ± 2.6	−22.8 ± 1.5	0.49	10.4	4.5 ± 0.3	1.3 ± 0.2	0.15
6SK:FDS_b	1.3 ± 1.2	−12.4 ± 0.8	0.51	30.7 ± 2.3	−27 ± 1.3	0.61	3.7	4.2 ± 0.4	1.3 ± 0.2	0.11
Mean:FDS_b		−13.0 ± 0.8		32.5 ± 2.5			7.1		1.3 ± 0.2	
5AB:T_m:FDS	3.9 ± 1.2	−14.6 ± 0.5	0.79	34.5 ± 2.8	−25.3 ± 1.1	0.69	9.2	4.5 ± 0.4	1.3 ± 0.1	0.27
6SK: T_m:FDS	2.7 ± 1.4	−14.8 ± 0.7	0.62	28.8 ± 2.5	−23.7 ± 1.3	0.56	5.1	4.2 ± 0.4	1.1 ± 0.2	0.11
Mean:T_m:FDS		−14.7 ± 0.6		31.7 ± 2.7			7.1		1.2 ± 0.2	
5AB:T_x:FDS	10.0 ± 1.3	−15.8 ± 0.5	0.79	38.9 ± 4.2	34.1 ± 1.7	0.64	73.0			
6SK:T_x:FDS	8.7 ± 1.4	−16.2 ± 0.7	0.66	54.9 ± 4.1	18.9 ± 2.1	0.23	73.8			
Mean:T_x:FDS		−16.0 ± 0.6								
5AB:T_n:FDS	−2.2 ± 1.2	−13.4 ± 0.5	0.77	73.3 ± 4.1	8.8 ± 1.6	0.11	82.1			
6SK:T_n:FDS	−2.7 ± 1.6	−14.6 ± 0.8	0.55	83.6 ± 4.1	−4.7 ± 2.1	0.01	78.9			
Mean:T_n:FDS		−14.0 ± 0.7								

This linear coupling of mean temperature on monthly to seasonal time scales to fraction of days with snow cover is clearly of great importance in understanding cold season climate, as it explains much of the interannual variability. From a climate change perspective, as the winter climate warms and the number of days when the surface is snow covered decreases, this gives a direct way of estimating the mean surface climate response. Specifically, we can expect that over the Prairies, a 10% drop in the number of days with snow cover will lead to warming of the cold season climate between 1.3 and 1.5°C.

5. Change of Cloud Coupling to the Diurnal Cycle Across Snow Transitions

Betts et al. [2013a] showed that the coupling between the diurnal climate and opaque cloud fraction had rapid transitions in November and March between two distinct states: warm season from April to October dominated by SWCF and a winter cold season from December to February dominated by LWCF. By stratifying the snow transition data from sections 3.1 and 3.2 by the daily mean opaque cloud cover across the snow transitions, we can show that these climate transitions actually occur in 5 days or less across the snow transitions.

5.1. Fall-Winter Transitions With Snowfall

Figure 7 takes the 15 days before and after snowfall for five Saskatchewan stations (Estevan, Moose Jaw, Regina, Saskatoon, and Swift Current) and bins the daily data by opaque cloud cover, after separating the data into 5 day bands, three before, and three after snowmelt, as shown in the figure legends. There are 216 fall-winter snow transitions, and not all of them are completely snow free for 15 days before and have snow cover lasting for the 15 days after. So we filtered to remove a small number of days (8%) to ensure that all days before the transition are snow free, and all days after the transition had snow cover. We still have about 6000 days in this analysis, which is sufficient for the stratification by opaque cloud, as it gives about 100 days in each subclass.

Figure 7 (first column) shows T_m, T_x, and T_n, color coded with red on the warm side ahead of the transition, black for the 5 day group just ahead of the snow transition, and blue with snow cover. T_x falls with increasing cloud, while T_n is flat in the period 5 to 15 days ahead of the transition. This is the warm season coupling between the diurnal cycle and cloud cover, when the SWCF dominates [*Betts et al.*, 2013a, Figure 9]. With snowfall, temperatures plunge, as the impact of clouds on SW_{net}, is sharply reduced by the large increase of surface albedo with snow (see section 7 later). Now the LWCF dominates [*Betts et al.*, 2013a], and T_n becomes colder with decreasing cloud, because the Earth can cool to space under clear skies. The downward transition between the warm season state and the winter state with snow takes 5 days or less. The fall of temperature of 10°C shown in Table 2 for Saskatchewan corresponds to a climatological cloud cover of 49% before and 58% after snowfall, but if cloud cover is small before and after snowfall, then the fall of maximum temperature reaches 20°C.

Figure 7 (second column) shows (top) RH_m, (middle) Q (heavy lines) and P_{LCL} (corresponding light lines) at the time of maximum temperature T_x (with only four time slices shown), and (bottom) ΔRH, the difference in RH between T_x and T_n. The warm season state shows the large diurnal range with high LCL at low cloud cover at the time of the afternoon T_x, characteristic of a deep convective BL [*Betts et al.*, 2013a]. Again, the transition is rapid to the cold season state where ΔRH is small, and RH varies much less with cloud cover and increases

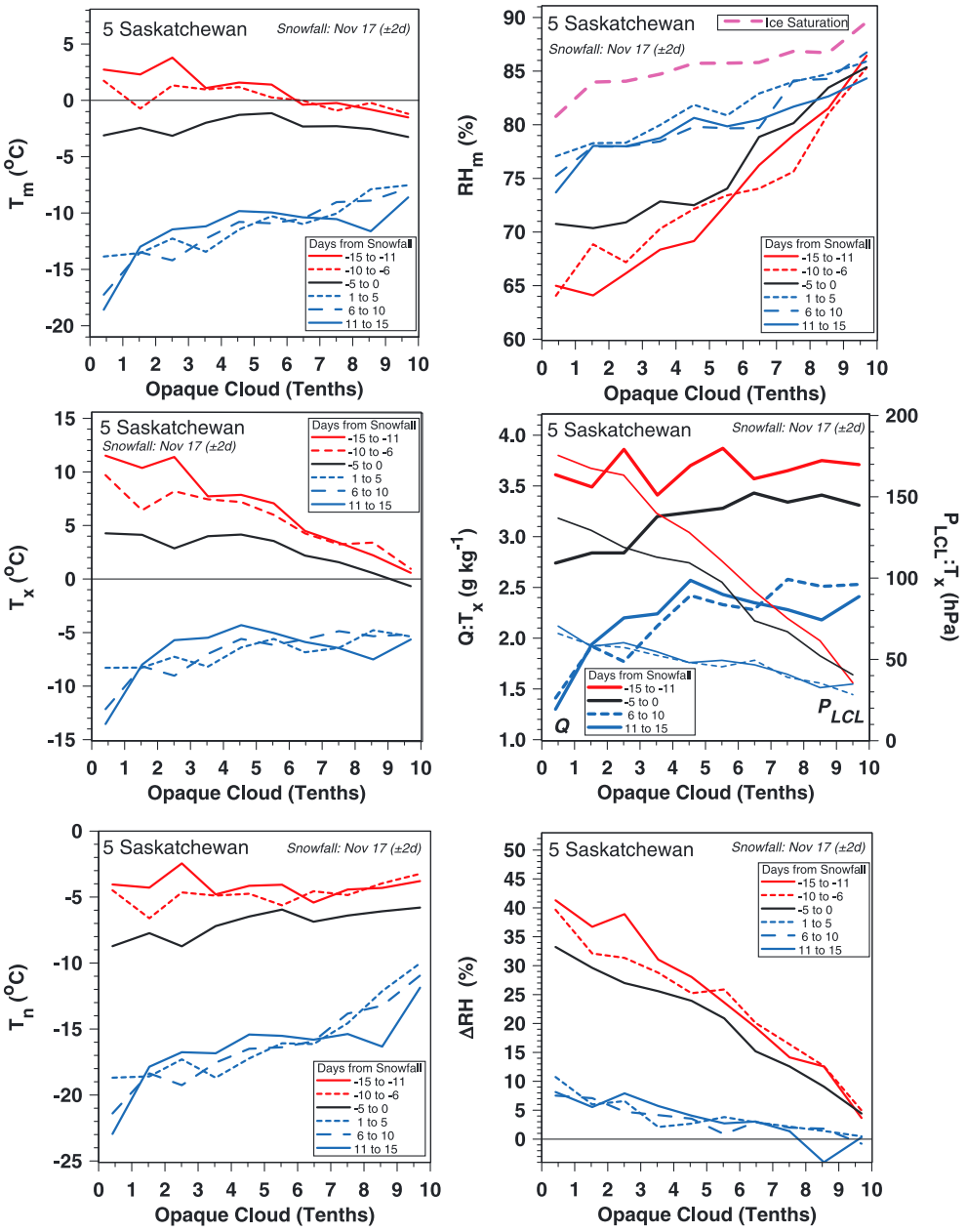

Figure 7. Coupling between cloud cover and surface climate across fall-winter snow transitions.

toward ice saturation (shown in Figure 7 (top) for T_n for days 6–15). Q and P_{LCL} are much smaller than their warm season values. The reduced saturation vapor pressure over ice can remove water vapor from the BL.

5.2. Winter-Spring Transitions Through Snowmelt

Figure 8 is the corresponding figure for the same stations for the transition through snowmelt in the spring. We filtered 6% of the days to ensure that all days before the transition had snow cover, and all days after the transition are snow free. Figure 8 (first column) for T_m, T_x, and T_n shows that the transition in the cloud coupling, which is now upward, occurs in the final five days of melt. After melt, T_x and T_m decrease as cloud cover increases, while T_n increases slightly. However, 5 to 15 days before melt, T_m, T_x, and T_n all decrease under clearer skies. Figure 8 (second column) shows the shift from cold to warm season states in the RH, Q, and P_{LCL} coupling to cloud with the reverse progression to Figure 7.

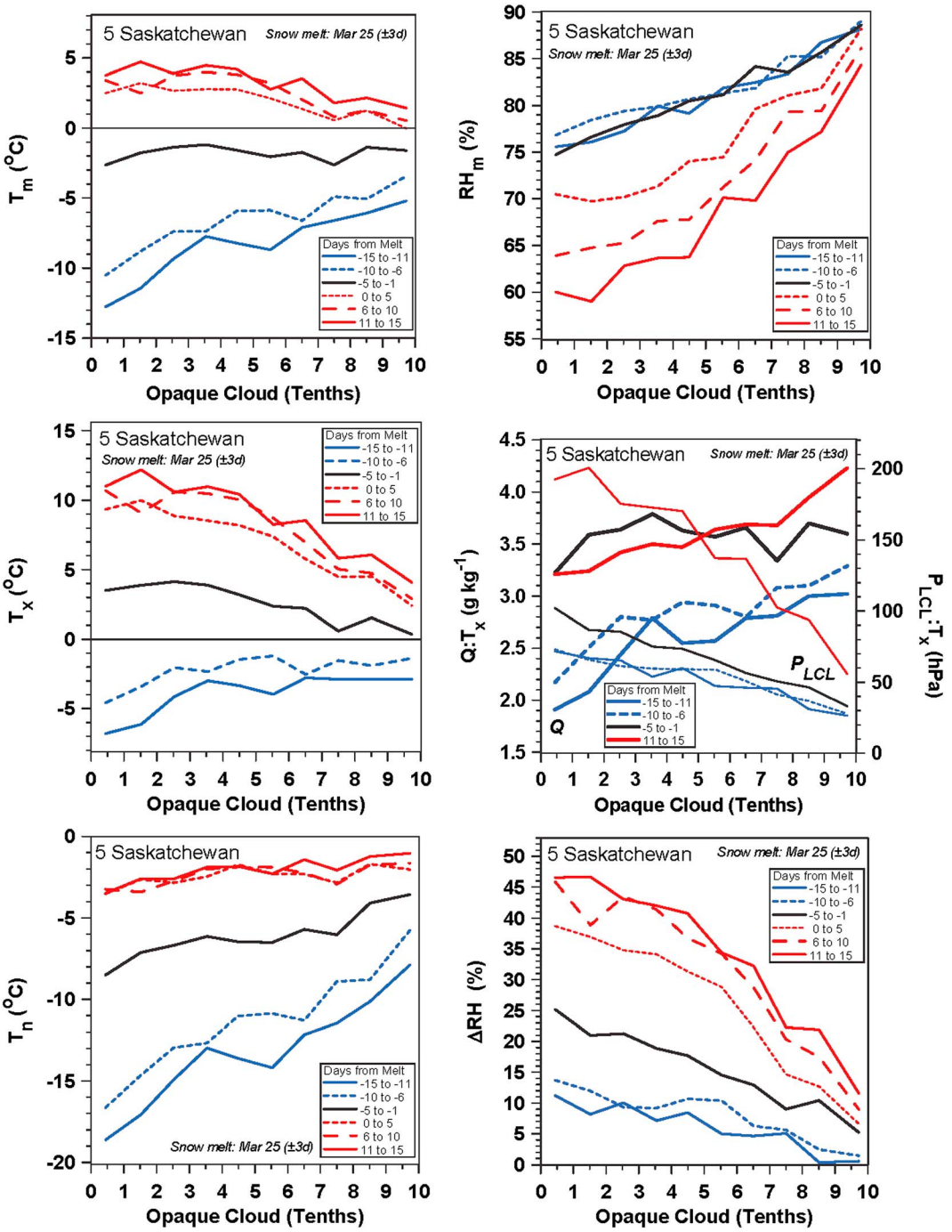

Figure 8. Same as Figure 7 but for the winter-spring transitions with snowmelt.

5.3. Discussion of Cloud Coupling Across Snow Transitions

Comparing Figures 7 and 8, we see small differences. Temperatures are slightly warmer and RH is slightly lower after snowmelt in early April than before snowfall in early November. This is consistent with the smaller solar zenith angle in April. With snow, minimum temperatures are also colder in late November than in early March, but the weak variation of RH with cloud cover is similar. However the rapid transitions with snow are very similar. They suggest that snow cover acts as a climate switch that drives a rapid shift in the diurnal cycle climate between a cold season state where LWCF dominates and a warm season state where SWCF dominates, as discussed by *Betts et al*. [2013a]. The warm season state has a strong diurnal cycle, driven by daytime solar forcing

generating a convective BL that can reach 180 hPa (1700 m) above the surface with clear skies. But with snow cover reducing SW_{net}, daily mean R_{net} becomes negative [*Betts et al.*, 2013a], and the surface cools and may uncouple from the atmosphere under a stable BL. The next sections will address the change in shortwave albedo with snow, the impact of snow on the downwelling longwave, and the surface radiation budget.

6. Coupling of Snow Cover to Surface Shortwave Albedo

The large changes in temperature across the snow transitions are driven by the large change in the surface albedo with snow, which we derived from a satellite-based product, produced by the Canada Centre for Remote Sensing (CCRS). The Canadian region extends from 40°N with a spatial resolution of 250 m and a temporal sampling rate of 10 days. There is also an Arctic circumpolar albedo product.

6.1. Surface Albedo Data

Surface albedo was estimated from the Moderate Resolution Imaging Spectroradiometer (MODIS) onboard the Terra satellite, which provides global coverage every 1–2 days in 36 spectral bands ranging from visible to infrared and to thermal wavelengths between 405 and 14,385 nm. The data are available since 2000. For the estimation of surface albedo, the first seven spectral bands of B1 to B7 ranging from 459 nm to 2155 nm were used. The MODIS 500 m land bands of B3 to B7 are downscaled to 250 m using an adaptive regression and normalization scheme [*Trishchenko et al.*, 2006]. To obtain clear-sky observations from MODIS, composite images for a 10 day period were generated by using a series of advanced algorithms [*Luo et al.*, 2008]. The 10 day composites of B1-B7 reflectance were then used to retrieve spatially continuous spectral albedo by using a combined land/snow BRDF (bidirectional reflectance distribution function) model. In that method, the modified RossThick-LiSparse BRDF model [*Luo et al.*, 2005; *Maignan et al.*, 2004] for land and the model of *Kokhanovsky and Zege* [2004] for snow are linearly combined for mixed surface conditions. They are weighted by snow fraction in the range 0.0 to 1.0. The seven spectral albedo values were then converted into one broadband surface albedo value, which represents the overall solar short-wave albedo, by using the empirical MODIS polynomial conversion equation of *Liang et al.* [1999]. The surface albedo product is in a Lambert conformal conic projection [*Khlopenkov and Trishchenko*, 2008] with a 250 m pixel resolution, and it is normalized to the local solar noontime for each pixel.

For our analysis, we computed a mean albedo on a 50 km × 50 km grid by averaging the 250 m pixels within a 200 × 200 window, for each 10 day composite of surface albedo. Note that the compositing process selects the date with the best atmospheric conditions, so the window 1–10 September may have data from any date in the 10 day window from 1 September 2000 to 10 September 2000. Any contaminated pixels (e.g., with cloud and cloud shadows) were excluded from this mean albedo calculation. As a result, a 50 km × 50 km grid may have fewer effective pixels in winter than in summer for the albedo mean due to more cloud cover [see *Betts et al.*, 2013b] and the possible misclassification of snow as cloud in winter. However, only 4% of the grid boxes have less than 50% of the total possible number of pixels (40,000).

6.2. Albedo and Climate Station Snow Depth

Using latitude and longitude for the center pixel of each 200 × 200 window, we selected the four grid boxes that enclosed the latitude-longitude for each climate station and generated a time sequence every 10 days of mean albedo for this 100 × 100 km domain. Figure 9 compares this mean albedo over the winter of 2000–2001 with the daily snow depth at the nine Prairie stations. The vertical lines are the boundaries of the surface snowpack. Overall, there is an excellent coherence between the point measurements of snow depth at the climate stations and this CCRS MODIS surface albedo on the 100 × 100 km scale.

The first snowfall of the season shows a sharp rise of albedo from values around 0.2 to 0.7 for the Prairie sites in Saskatchewan and Manitoba. Surface albedo stays high until snowmelt. The snow transitions are marked by an increase in the standard deviation across the four 50 km grid boxes and the standard deviation within each 50 km grid (not shown), because of the rapidly changing fraction of snow cover across the landscape and the large differences in albedo between snow and bare soil. Albedo at Prince Albert on the edge of the boreal forest is a little lower, and the larger variance reflects the strong north-south gradient of albedo on the 100 km scale. At The Pas within the boreal forest, albedo is lowest, closer to 0.1 with no snow and reaching only 0.4 to 0.5 with snow in midwinter. Figure 9 (bottom row) for the three Alberta stations shows the large fluctuations of winter albedo with episodic melt of the snowpack.

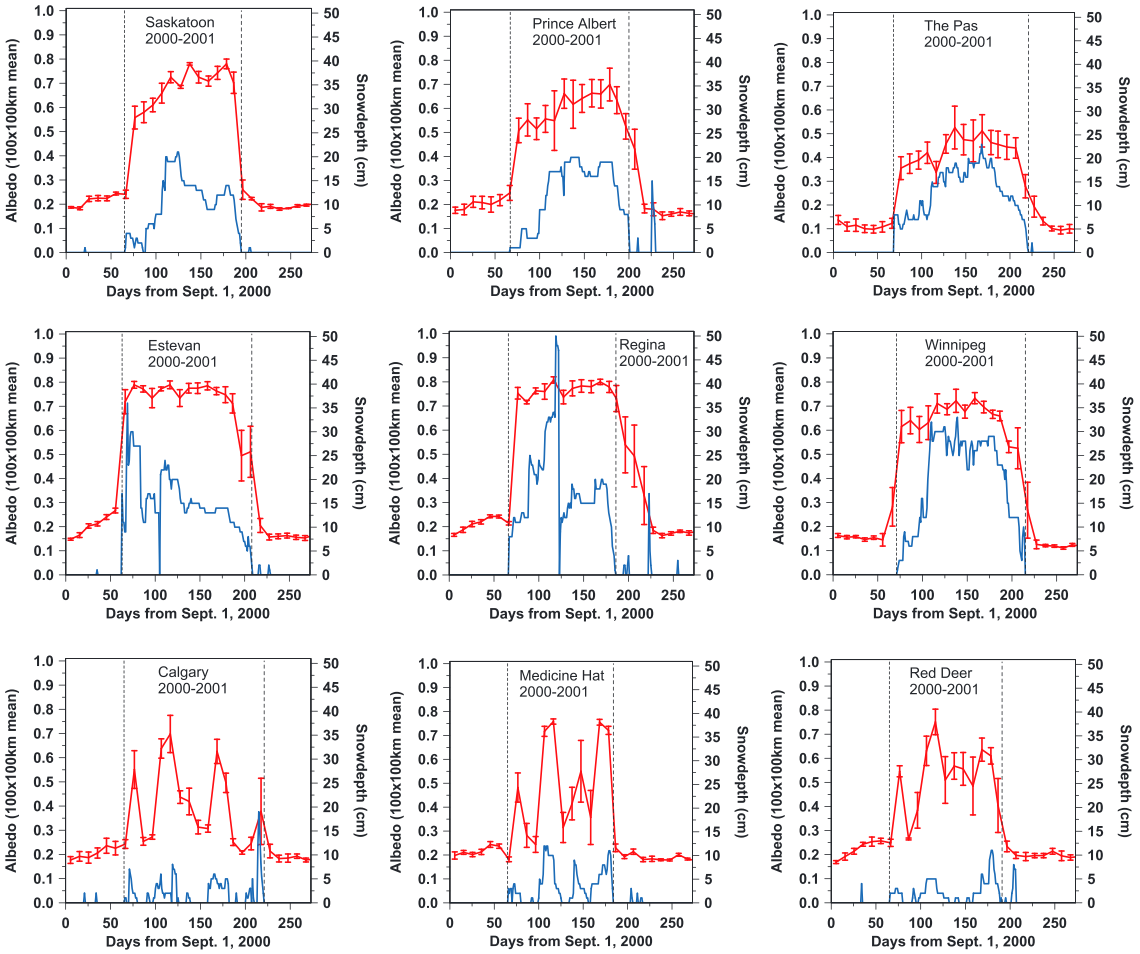

Figure 9. Comparison of station snow depths (blue) with 100 × 100 km MODIS albedo (red) from September to May.

When snow depths are shallow, the landscape may not be covered uniformly, and together with the blowing of snow on the Prairies [*Pomeroy et al.*, 1993], this will reduce mean albedo. We see lower albedo, of order 0.5–0.6, around Saskatoon and Prince Albert in December 2000 when recorded snow depth is ≈5cm.

6.3. North-South Cross Section of Surface Albedo

Figure 10 shows a north-south cross section of mean albedo for the winter of 2000–2001 through central Saskatchewan between 104°W and 108°W. There are about twelve 50 km grid boxes averaged in each 1° latitude band. Surface albedo over the Prairies with snow is on the order of 0.7. The latitude band 49–50°N has slightly lower albedo, because there is partial melt of some southern grid boxes (not shown). Over the boreal forest between 54 and 55°N, albedo is on the order of 0.1 without snow and 0.35 with snow.

The latitudinal transition is rapid: the grid boxes in the band from 53 to 54°N contain both agricultural land and boreal forest (not shown), giving the intermediate mean albedo shown. Note that the area mean albedo values for the boreal forest are larger than those measured at individual flux towers during BOREAS [*Betts and Ball*, 1997], because the landscape includes snow covered wetlands and lakes as well as forest, where the trees shade the snow.

7. Change in the Surface Radiation Budget Across Snow Transitions

Snow lying on the surface has several impacts on the surface energy balance [*Cohen*, 1994; *Betts*, 2011]. The first is the increased surface albedo: increased reflection reduces SW_{net}. The large cooling we have seen in

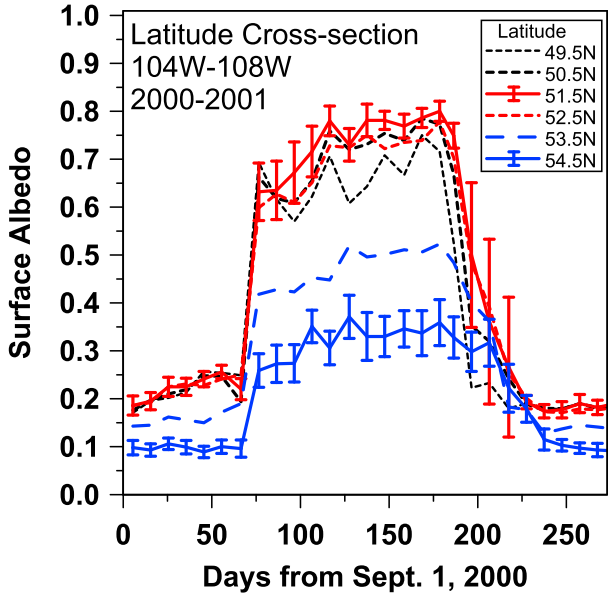

Figure 10. North-south cross section of albedo for winter period 2000–2001.

section 3 with snow cover drives a shift from an unstable convective BL with clouds to a stable BL. The second is that with temperatures below freezing, transpiration ceases, and the reduced saturation vapor pressure over ice removes water vapor from the BL and reduces sublimation. On regional scales, this can reduce atmospheric water vapor, and this reduction, along with the cooling of the atmosphere, will reduce the clear-sky LW_{dn}. However, we have seen that the mean cloud cover generally increases with snow cover, because the number of days with overcast conditions increases, and this reduces both the SW heating and the LW cooling of the surface. A fourth factor is that a layer of surface snow insulates the ground and reduces the ground heat flux, but we will not address this here.

7.1. Surface Radiation Budget

The surface net radiation, R_{net}, can be expanded in terms of the net shortwave and longwave fluxes, SW_{net} and LW_{net} and their components, the upward and downward fluxes (suffixes: up and dn)

$$R_{net} = SW_{net} + LW_{net} = (SW_{dn} - SW_{up}) + (LW_{dn} - LW_{up}) \quad (4)$$

Opaque clouds reduce the downward shortwave flux, SW_{dn}, below its clear-sky value, SW_{dn}(clear). This is expressed as the surface shortwave cloud forcing, SWCF, defined negative as

$$SWCF = SW_{dn} - SW_{dn}(clear) \quad (5)$$

Betts and Viterbo [2005] and *Betts* [2009] defined an effective cloud albedo, ECA, as

$$ECA = -SWCF \ / SW_{dn}(clear) \quad (6)$$

This is a dimensionless measure of the fraction of SW_{dn}(clear) that is reflected or absorbed by the cloud field per unit area of the surface. This removes the seasonal change in the clear-sky flux. This effective cloud albedo plays a similar role to the surface albedo (α_s) in the surface energy balance, since the net shortwave flux can be written as

$$SW_{net} = (1 - \alpha_s)(1 - ECA)\ SW_{dn}(clear) \quad (7)$$

where

$$\alpha_s = SW_{up} \ / \ SW_{dn} \quad (8)$$

For the change of the surface albedo, α_s, with snow cover, we will use the MODIS data from section 6.

We will use the fits for SW_{dn}(clear), derived by *Betts et al.* [2013a] as a function of latitude, from SW_{dn} measurements at Lethbridge, Swift Current, The Pas, and Winnipeg and data from the BOREAS and one of the Boreal Ecosystem Research and Monitoring Sites (BERMS) sites. These simplified fits as a function of day of year (DOY), which have no dependence on aerosol or atmospheric water vapor, are

$$SW_{dn}(clear) = A + B * COS(\pi * (DOY - 170)/365))^2 \quad (9)$$

where the coefficients (A and B) are (68 and 321) at 49.92°N, (54, 324) at 52.16°N, and (42, 326) at 53.97°N.

We will also use the simplified fit between opaque cloud cover and ECA (which has no dependence on cloud height distribution or cloud structure), derived by *Betts et al*. [2013a] for the cold winter period, November to February

$$\mathrm{ECA} = 0.1056 + 0.0404\ \mathrm{OpaqueCloud} + 0.00158\ \mathrm{OpaqueCloud}^2 \tag{10}$$

Opaque clouds also increase the down-welling longwave flux, LW_{dn}, giving a positive longwave cloud forcing defined as

$$\mathrm{LWCF} = \mathrm{LW_{dn}} - \mathrm{LW_{dn}(clear)} \tag{11}$$

In section 7.3, we will estimate the impact of opaque clouds and snow cover on LW_{dn}. In section 7.4, we will estimate changes in LW_{up} from changes in surface radiometric skin temperature, T_{sk}, using

$$\mathrm{LW_{up}} = \sigma\,(273.15 + \mathrm{T_{sk}})^4 \tag{12}$$

where $\sigma = 5.67 * 10^{-8}$, and the emissivity is set to 1.

7.2. Surface Shortwave Albedo

Based on Figure 10, we estimated a representative value of shortwave albedo for the snow covered central Prairies for the transition through winter, by averaging the (36) 50 km grid boxes between 50–53°N and 104–108°W, giving

$$\text{September} - \text{October} : \alpha_s = 0.22 \pm 0.03$$

$$\text{December} - \text{February} : \alpha_s = 0.73 \pm 0.07$$

$$\text{21 April to 31 May} : \alpha_s = 0.18 \pm 0.02$$

Albedo is slightly higher in the fall before snowfall than in the spring after snowmelt. Soil after snowmelt is wet and darker, while dry plant residue before snowfall has a higher reflectance [*Nagler et al*., 2000].

We computed comparable numbers for the four 50 km grid boxes that surround the boreal forest station of The Pas, giving

$$\text{15 September to 31 October and 1–31 May} : \alpha_s = 0.10 \pm 0.2$$

$$\text{December} - \text{February} : \alpha_s = 0.44 \pm 0.08$$

7.3. Change in LW_{dn} Across Snow Transitions

We have a 10 year record of LW_{dn} in the Prince Albert National Park from BOREAS and BERMS. *Betts et al*. [2013a] paired these data with the climate station data at Prince Albert (at a distance of 57 km) to show the coupling between LW_{net} and opaque cloud data. Here we selected the 15 days before and after the snow transitions in both fall and spring and binned the days against opaque cloud in tenths, subsetting by the presence or absence of surface snow. In fall, we included all the transitions, where snow lasted a week or more (402 days total); in spring, there is a single snowpack melt transition for each year (300 days total).

Figure 11 shows the change of LW_{dn} across these snow transitions, plotted against opaque cloud cover. LW_{dn} increases with cloud cover as expected, as the LWCF increases, but it also falls on average by 22 Wm^{-2}, for the same cloud cover, if there is snow on the surface. We will use the two linear fits shown to represent the coupling of LW_{dn} to opaque cloud and snow. With a single station and only 10 years of data, we do not have sufficient data to estimate error bars for these fits.

$$\mathrm{LW_{dn}} : \mathrm{NoSnow} = 223.7 + 7.7 * \mathrm{OpaqueCloud} \tag{13a}$$

$$\mathrm{LW_{dn}} : \mathrm{Snow} = 202.4 + 7.5 * \mathrm{OpaqueCloud} \tag{13b}$$

The surface T_m falls in response to this drop of LW_{dn} and the drop of SW_{net}, coming from greatly increased albedo with snow.

7.4. Estimate of the Drop in the Surface Radiative Temperature Across Fall Snow Transition.

For this, we neglect changes in the sum of the surface sensible, latent, and ground heat fluxes across the fall snow transition, which is equivalent to neglecting the change of net radiative flux. Putting together just the radiative components, we can roughly estimate the drop of surface temperature required to cancel the drop in SW_{net} from equation (7) and the drop of LW_{dn} from equation (13) across the fall snow transition. We use the

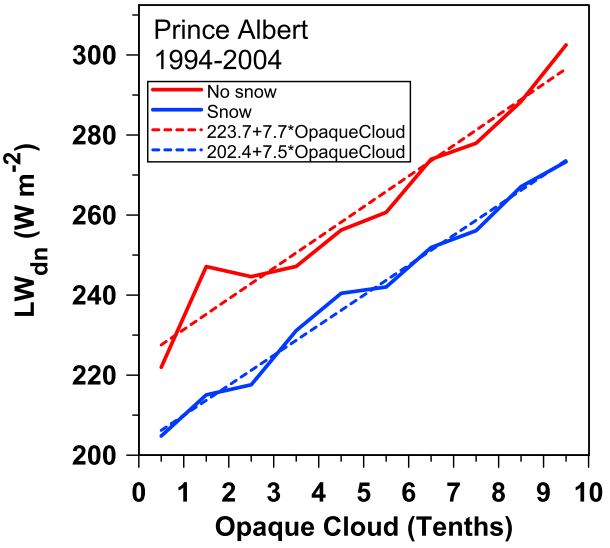

Figure 11. Change in LW_{dn} across snow transitions as a function of opaque cloud cover.

6-Saskatchewan composite for the mean fall transition in Table 2 to generate the idealized radiation budget in Table 6. The first line is for snow-free conditions with $\alpha_s = 0.22$ and opaque cloud cover of 49%. The second line is with $\alpha_s = 0.73$ and observed cloud cover of 58 % with snow, which increases the ECA using equation (10) from 0.33 to 0.38. The third line is for $\alpha_s = 0.73$ with snow and no change of cloud cover. We show this so the impact of the cloud cover change on the partly canceling SWCF and LWCF can be seen.

Using equation (9) for SW_{dn}(clear) with coefficients (A and B) = (58, 323) for 51.5°N, for the fall months of October, November, and December, gives mean SW_{dn} (clear) = 97.2 Wm^{-2}. The fall in SW_{net} across the snow transition is 34.0 Wm^{-2} with the observed cloud increase and slightly less 32.7 Wm^{-2}, if there were no cloud cover change. Using equation (13) with the increase in cloud cover across the snow, transition gives a fall of LW_{dn} of 15.4 Wm^{-2} and a larger value of 22.1 Wm^{-2}, again with no change in cloud cover. This gives a total fall in these surface radiative heating terms of 49.4 Wm^{-2} with the observed change of cloud cover and a larger value of 54.8 Wm^{-2} without a cloud cover change. Note that the LWCF change of +6.7 Wm^{-2} is greater than the cloud impact on SW_{net}, which is only −1.3 Wm^{-2}, because the high surface albedo in equation (7) reduces the impact of the SWCF and ECA from equation (6).

The drop, ΔT, in the T_{sk} needed to balance these reductions in radiative forcing is −11.4 K for the observed transition, which is only slightly larger than the values in Table 2 of $\Delta T_m = -9.6 \pm 0.8$ for the Saskatchewan composites and -10.7 ± 0.8 for the Manitoba composites. No change in cloud cover would give a slightly larger estimate of $\Delta T = -12.7$ K. So for the observed fall transition, which involves both an increase in surface albedo and opaque cloud cover, 69% of the decrease of 49.4 Wm^{-2} in radiative forcing comes from a drop in SW_{net} and 31% from a drop of LW_{dn}.

The bottom two lines in Table 6 use the fall snow transition data for The Pas, a station within the boreal forest, where the increase in α_s is from 0.1 to 0.44, and the opaque cloud increase is from 61 to 71%. Here we see that the smaller change in the surface radiative forcing would drive a surface cooling of $T_{sk} = -7.7$ K, smaller than the Prairies in Saskatchewan. This is however the drop in T_m seen for the fall-winter snow transitions for The Pas, one of the two Manitoba stations in Table 2.

In spring, the larger SW_{net} is first melting the snowpack and then melting soil ice and warming the soil, so the energy budget is more complex, and we do not have the data to estimate the terms.

8. Shortwave Forcing of the Winter Diurnal Cycle

We have addressed the large changes in land-surface climate that occur with snow cover as a result of the increased albedo reducing SW_{net}. One further consequence is a large reduction in the shortwave forcing of

Table 6. Idealized Surface Radiation Budget

Data	SW_{dn}(clear)	α_s	Cloud	ECA	SW_{net}	LW_{dn}(13)	LW_{net}	R_{net}	T_{sk}	ΔT
Units	(Wm^{-2})		(%)		(Wm^{-2})	(Wm^{-2})	(Wm^{-2})	(Wm^{-2})	(K)	(K)
6SK-Fall	97.2	0.22	49	0.33	50.0	261.3	−54.3	−4.4	273.2	0
6SK-Fall	97.2	0.73	58	0.38	16.0	245.9	−22.3	−4.4	261.8	−11.4
6SK-Fall	97.2	0.73	49	0.33	17.3	239.2	−22.6	−4.4	260.5	−12.7
The Pas-Fall	81.5	0.10	61	0.41	43.3	270.5	−45.1	−1.8	273.15	0
The Pas-Fall	81.5	0.44	71	0.47	24.1	255.7	−26.0	−1.8	265.48	−7.7

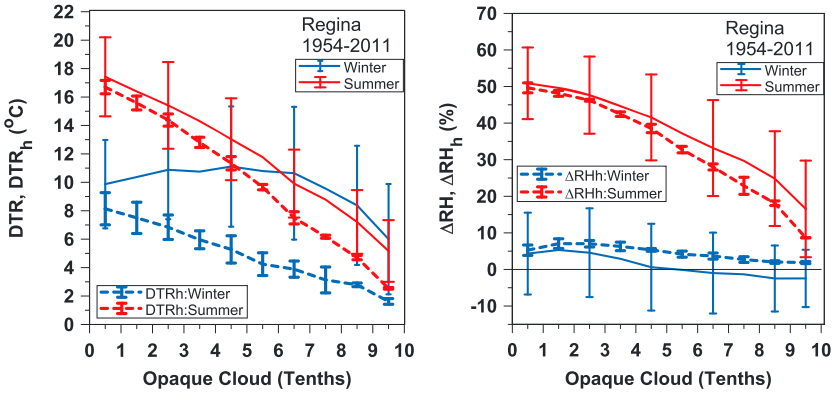

Figure 12. The difference of cloud coupling for the mean diurnal climate and the monthly mean diurnal climate for Regina.

the diurnal cycle. This leads to an important difference between the mean diurnal climate and the mean monthly diurnal climate (Wang and Zeng, in revision, 2013), because temperature advection on daily time scales is typically larger than the solar-forced diurnal temperature range. (Wang and Zeng, in revision, 2013) show that averaging up to the monthly time scale extracts the relatively small radiatively forced diurnal temperature signal. The rapid climate transitions with snowfall are necessarily coupled to advective changes, but the monthly averages binned by opaque cloud transform the picture of the diurnal temperature range in winter.

In addition to

$$DTR = T_x - T_n \quad (1)$$

where T_x and T_n are simply the conventional daily maximum and minimum temperatures, (Wang and Zeng, in revision, 2013) define

$$DTR_h = T_{xh} - T_{nh} \quad (14)$$

where T_{xh} and T_{nh} are the maximum and minimum air temperature values derived from the monthly mean diurnal cycle of temperature. We will also define

$$\Delta RH_h = RH_{xh} - RH_{nh} \quad (15)$$

where RH_{xh} and RH_{nh} are the maximum and minimum RH values derived from the monthly mean diurnal cycle of RH.

Since opaque cloud cover is related to ECA through equation (10) and hence SW_{net} through equation (7), the stratification by opaque cloud cover is related to SW_{net}. Figure 12 compares the summer (June, July, and August) and winter (December, January, and February) means of the daily DTR and ΔRH and their daily standard deviations, with the average summer and winter DTR_h and ΔRH_h derived from the monthly mean diurnal cycle for each cloud bin, where the standard deviation shown is between the 3 months.

The standard deviations of the DTR daily values (Figure 12, left) are similar in winter and summer at low cloud cover, but as cloud increases the winter daily variability gets much larger than in summer. This is consistent with the conclusion of (Wang and Zeng, in revision, 2013) that in winter, $DTR = T_x - T_n$ is dominated by the large variations in daily temperature advection, and it is not a useful measure of the diurnal cycle forced by the reduced solar heating. In contrast to the nonlinear behavior of DTR in winter, DTR_h has a monotonic decrease with decreasing solar forcing (increasing cloud cover) and falls to 1.6°C when cloudy. Because we have more than 55 years of data, there are more than 100 days in each monthly mean diurnal cycle for each cloud bin, and this easily extracts the diurnal signal from the advective variability that is not diurnally coupled. In summer, DTR and DTR_h show a similar monotonic decrease with increasing cloud cover, with the difference DTR-DTR_h increasing with cloud cover. This is consistent with the fact that the timing of daily T_x and T_n is affected by advection, whereas in the monthly mean, T_n is at sunrise and T_x generally midafternoon [see *Betts et al.*, 2013a, Figure 3].

Figure 12 (right) shows a similar small difference in summer between ΔRH, which is the difference between RH at T_n and T_x, and ΔRH_h, which is a true diurnal range of RH in the monthly mean diurnal cycle, stratified by

opaque cloud. The standard deviations of the daily ΔRH are similar in summer and winter, but in winter, the standard deviation is far larger than the mean. In contrast, ΔRH_h in winter decreases with increasing cloud and has a very small standard deviation between the three winter months.

We conclude that in winter, the monthly mean diurnal climate shows a nearly linear dependence on the reduced shortwave forcing, but the mean diurnal climate does not. However, we were not able to construct a satisfactory energy budget as a function of cloud cover for the stable BL regime in winter. The high solar zenith angle and high surface albedo reduce SW_{net}, and LW_{net} depends critically on the radiometric surface T_{sk}. Under clear skies, the difference $T_{sk} - T_m$ can become large at night [*Lesins et al*., 2012], and we have no measurements of T_{sk}. Warming a shallow stable BL with a depth of order 100 m at a rate of 1°C/h^{-1} requires a net flux of only 20 Wm^{-2}, which is comparable to the large uncertainty in R_{net}.

9. Conclusions

By compositing surface data from 13 climate stations across snow events, we have shown the rapid changes in the surface climate over the Canadian Prairies that occur with the winter and spring transitions with snow. We conclude that snow cover acts as a fast climate switch. With fresh snowfall, air temperature near the surface falls within 5 days by about 10 K and rises by a similar amount across snowmelt over 1 to 3 weeks. The diurnal range of RH drops to <10% with snow cover, as RH rises toward saturation over ice. This is a very robust climate signal in the fall, winter, and spring seasons. On monthly to seasonal time scales, there is a quasi-linear coupling of mean temperature to fraction of days with snow cover, with mean temperature falling with each 10% increase in days with snow cover by 1 K in fall and spring and by 1.3 to 1.5 K for the entire cold season including winter. As much as 70% of the interannual variability of the October to April mean temperature is associated with the fraction of days with snow cover.

This quasi-linear coupling of mean temperature on the seasonal time scales to the fraction of days with snow cover is clearly of great importance in understanding cold season climate. From a climate change perspective, as the winter climate warms and the number of days when the surface is snow-covered shrinks, this gives a direct way of estimating the mean surface climate response. Specifically, we can expect that over the Prairies, a 10% drop in the number of days with snow cover will lead to warming of the mean winter climate by about 1.4°C.

The change in surface shortwave albedo from ≈0.2 to ≈0.7 with snow cover on the Prairies is a fast climate process that is tightly coupled to these winter transitions. On global scales, this is well known as snow-ice albedo feedback, but the coupled physics operates within a few days on regional scales over land. The traditional surface climatological view that cold regions have more snow gives insufficient recognition to the coupled positive feedback that lead to a rapid fall of the surface temperature with snow cover. As well as shortwave reflection, snow on the surface is an insulator that reduces the upward ground heat flux, and the low saturation vapor pressure over ice removes water vapor from the atmosphere and reduces sublimation, which together with colder temperatures reduces the LW_{dn} flux, the water vapor greenhouse effect. However, we also saw a small increase in opaque cloud cover with snow cover, corresponding to an increase in effective cloud albedo on the order of 5%. This has opposite impacts on the SWCF and LWCF, but with snow cover increasing the surface albedo and reducing SW_{net}, the LWCF dominates.

Betts et al. [2013a] showed that the coupling between the diurnal climate and opaque cloud fraction had rapid transitions in November and March between two distinct states: warm season from April to October dominated by SWCF and a winter cold season from December to February dominated by LWCF. Here we refine this picture further by comparing the rapid fall transitions in temperature and humidity that occur with snowfall with the October to December climatology. In essence, the 30 day transition in the fall climatology occurs within 5 days, coupled to major snow events, whose date varies by ±15 days.

By compositing the changes across the fall and spring snow transitions against opaque cloud cover, we showed that snow cover acts as a fast climate switch that drives a rapid shift in the diurnal cycle climate between a warm season state with a deep convective BL, where SWCF dominates and near-surface temperatures fall under cloudy skies, and a cold season state with a stable BL, where LWCF dominates and near-surface temperatures fall under clear skies.

We calculate the change in the surface radiative budget with snow using the surface albedo data from the MODIS and station longwave data. We find that with fall snow transitions, the surface radiative heating is reduced by 50 Wm^{-2}, with 69% coming from the reduced net shortwave flux, resulting from the increased surface albedo and a small increase in effective cloud albedo, and 31% from a reduced incoming longwave flux with snow cover. This drop in surface radiative heating is sufficient to drive a drop in the surface radiometric skin temperature of 11 K.

The corresponding calculation for The Pas, a station within the boreal forest, where the mean surface albedo changes from 0.1 to 0.44 with winter snow cover, suggests that the radiative change could drive a fall of $T_{sk} \approx 7.7$ K. The fall-winter snow transitions at The Pas show a similar value, while the winter-spring transitions and the fall and spring snow day climatologies at all three northern sites suggest that T_m changes by 10 K with snow cover. We plan to explore in a later paper the impact of snow transitions on temperature deeper within the boreal forest using data from BOREAS and BERMS.

We have confirmed the analysis of (Wang and Zeng, in revision, 2013) that in winter, the monthly mean diurnal temperature range shows a nearly linear dependence on the reduced shortwave forcing; but the conventional $DTR = T_x - T_n$ does not, because it is dominated by the large variations in daily temperature advection.

This analysis is based on surface data and addresses time scales from a few days with snowfall to the coupling of seasonal and winter variability to the fraction of days with snow cover. We have seen that the surface temperature cooling with snow cover increases from −10 K for the fall and spring transitions to nearly −15 K for winter variability on regional scales, presumably because of the coupling between the surface cooling, the troposphere, and the regional atmospheric flow [*Viterbo and Betts*, 1999]. From an agricultural perspective, snow cover reduces the coupling between air and soil, and this limits soil freezing. Moreover, the protection of winter crops from frost damage depends on snow depth [*Thorsen et al*., 2010; *Trnka et al*., 2010], whereas the drop of air temperature is dependent more on snow albedo than on snow depth. It is clear that the modeling of frost damage to crops as the winter climate warms and snow cover is reduced requires a fully coupled system.

The development and evaluation of improved representations of snow cover, surface albedo, and snow-albedo feedback in global models remain an important issue [*Melloh et al*., 2002; *Roesch and Roeckner*, 2006; *Qu and Hall*, 2007; *Wang and Zeng*, 2010; *Dutra et al*., 2010, 2012; *Xu and Dirmeyer*, 2013]. Our data come from a specific latitude-longitude zone (49–53°N, 97–114°W) in Canada with long homogeneous records, but we expect that our results will prove useful in evaluating the strength of snow-atmosphere coupling in regional and global models. We plan to make our reduced daily climate data set available for such studies.

Acknowledgments

This research was supported by Agriculture and Agri-Food Canada and by Atmospheric Research. We thank the civilian and military technicians of the Meteorological Service of Canada and the Canadian Forces Weather Service, who have made accurate cloud observations hourly for 60 years. We thank the Saskatchewan Research Council for the BOREAS radiation measurements and Alan Barr for maintaining the BERMS radiation measurements at the Old Aspen site. We thank three reviewers for their helpful suggestions.

References

Betts, A. K. (2004), Understanding hydrometeorology using global models, *Bull. Am. Meteorol. Soc.*, *85*, 1673–1688.

Betts, A. K. (2009), Land-surface-atmosphere coupling in observations and models, *J. Adv. Model Earth Syst.*, *1*, *Art. #4*, 18 pp., doi:10.3894/JAMES.2009.1.4.

Betts, A. K. (2011), Seasonal climate transitions in New England, *Weather*, *66*, 245–248, doi:10.1002/wea.754.

Betts, A. K., and J. H. Ball (1995), The FIFE surface diurnal cycle climate, *J. Geophys. Res.*, *100*, 25,679–25,693.

Betts, A. K., and J. H. Ball (1997), Albedo over the boreal forest, *J. Geophys. Res.*, *102*, 28,901–28,910.

Betts, A. K., and J. H. Ball (1998), FIFE surface climate and site-average dataset: 1987–1989, *J. Atmos. Sci.*, *55*, 1091–1108.

Betts, A. K., and P. Viterbo (2005), Land-surface, boundary layer and cloud-field coupling over the south-western Amazon in ERA-40, *J. Geophys. Res.*, *110*, D14108, doi:10.1029/2004JD005702.

Betts, A. K., R. Desjardins, and D. Worth (2013a), Cloud radiative forcing of the diurnal cycle climate of the Canadian Prairies, *J. Geophys. Res. Atmos.*, *118*, 8935–8953, doi:10.1002/jgrd.50593.

Betts, A. K., R. Desjardins, D. Worth, and D. Cerkowniak (2013b), Impact of land-use change on the diurnal cycle climate of the Canadian prairies, *J. Geophys. Res. Atmos.*, *118*, 11,996–12,011, doi:10.1002/2013JD020717.

Bony, S., et al. (2006), How well do we understand and evaluate climate change feedback processes?, *J. Clim.*, *19*, 3445–3482, doi:10.1175/JCLI3819.1.

Cess, R. D., et al. (1991), Interpretation of snow-climate feedback as produced by 17 general circulation models, *Science*, *253*, 888–892.

Cohen, J. (1994), Snow cover and climate, *Weather*, *49*, 150–156.

Cohen, J., and D. Rind (1991), The impact of the snow cover on the climate, *J. Clim.*, *4*, 689–706, doi:10.1175/1520-0442(1991)004<0689:TEOSCO>2.0.CO;2.

Dewey, K. F. (1977), Daily maximum and minimum temperature forecasts and the influence of snow cover, *Mon. Weather Rev.*, *105*, 1594–1597, doi:10.1175/1520-0493(1977)105<1594:DMAMTF>2.0.CO;2.

Dutra, E., G. Balsamo, P. Viterbo, P. M. A. Miranda, A. Beljaars, C. Schär, and K. Elder (2010), An improved snow scheme for the ECMWF land surface model: Description and offline validation, *J. Hydrometeorol*, *11*, 899–916, doi:10.1175/2010JHM1249.1.

Dutra, E., C. Schär, P. Viterbo, and P. M. A. Miranda (2011), Land-atmosphere coupling associated with snow cover, *Geophys. Res. Lett.*, *38*, L15707, doi:10.1029/2011GL048435.

Dutra, E., P. Viterbo, P. M. A. Miranda, and G. Balsamo (2012), Complexity of snow schemes in a climate model and its impact on surface energy and hydrology, *J. Hydrometeorol.*, *13*, 521–538, doi:10.1175/JHM-D-11-072.1.
Groisman, P. Y., T. R. Karl, and R. W. Knight (1994), Observed impact of snow cover on the heat balance and the rise of continental spring temperatures, *Science*, *263*, 198–200, doi:10.1126/science.263.5144.198.
Hall, A. and X. Qu (2006), Using the current seasonal cycle to constrain snow albedo feedback in future climate change. *Geophys. Res. Lett.*, *33*, L03502, doi:10.1029/2005GL025127.
Khlopenkov, K. V., and A. P. Trishchenko (2008), Implementation and evaluation of concurrent gradient search method for reprojection of MODIS Level 1B imagery, *IEEE Trans. Geosci. Remote Sens.*, *46*, 7.
Kokhanovsky, A. A., and E. P. Zege (2004), Scattering optics of snow, *Appl. Opt.*, *43*(20), 1589–1602, doi:10.1364/AO.43.001589.
Lesins, G., T. J. Duck, and J. R. Drummond (2012), Surface energy balance framework for arctic amplification of climate change, *J. Clim.*, *25*, 8277–8288, doi:10.1175/JCLI-D-11-00711.1.
Liang, S., A. Strahler, and C. Walthall (1999), Retrieval of land surface albedo from satellite observations: A simulation study, *J. Appl. Meteorol.*, *38*, 712–725.
Lott, B., and H.-F. Graf (1993), Snow cover model for global climate simulations, *J. Geophys. Res.*, *98*, 10,451–10,464.
Luo, Y., A. P. Trishchenko, R. Latifovic and Z. Li (2005), Surface bidirectional reflectance and albedo properties derived using a landcover based approach with MODIS observations, *J. Geophys. Res.*, *110*, D01106, doi:10.1029/2004JD004741.
Luo, Y., A. P. Trishchenko, and K. V. Khlopenkov (2008), Developing clear-sky, cloud and cloud shadow mask for producing clear-sky composites at 250-meter spatial resolution for the seven MODIS land bands over Canada and North America, *Remote Sens. Environ.*, *112*, 4167–4185.
Maignan, F., F. M. Bréon, and R. Lacaze (2004), Bidirectional reflectance of Earth targets: Evaluation of analytical models using a large set of spaceborne measurements with emphasis with the hot spot, *Remote Sens. Environ.*, *90*, 210–220.
Manual of Surface Weather Observations (MANOBS) (2013), Environment Canada MANOBS, Chapter 1, Sky. http://www.ec.gc.ca/manobs/default.asp?lang=En&n=A1B2F73E-1.
Melloh, R. A., J. P. Hardy, R. N. Bailey, and T. J. Hall (2002), An efficient snow albedo model for the open and sub-canopy, *Hydrol. Process.*, *16*, 3571–3584, doi:10.1002/hyp.1229.
Mote, T. L. (2008), On the role of snow cover in depressing air temperature, *J. Appl. Meteorol. Climatol.*, *47*, 2008–2022.
Nagler, P. L., C. S. T. Daughtry, and S. N. Goward (2000), Plant litter and soil reflectance, *Remote Sens. Environ.*, *71*, 207–215.
Namias, J. (1960), Snowfall over eastern United States: Factors leading to its monthly and seasonal variations, *Weatherwise*, *13*, 238–247, doi:10.1080/00431672.1960.9940990.
Namias, J. (1985), Some empirical evidence for the influence of snow cover on temperature and precipitation, *Mon. Weather Rev.*, *113*, 1542–1553, doi:10.1175/1520-0493(1985)113<1542:SEEFTI>2.0.CO;2.
Pomeroy, J. W., D. M. Gray, and P. G. Landine (1993), The prairie blowing snow model: Characteristics, validation, operation, *J. Hydrol.*, *144*, 165–192.
Qu, X., and A. Hall (2007), What controls the strength of snow-albedo feedback?, *J. Clim.*, *20*, 3971–3981.
Roesch, A., and E. Roeckner (2006), Assessment of snow cover and surface albedo in the ECHAM5 general circulation model, *J. Clim.*, *19*, 3828–3843.
Thorsen, S. M., A.-G. Roer, and M. van Oijen (2010), Modelling the dynamics of snow cover, soil frost and surface ice in Norwegian grasslands, *Polar Res.*, *29*, 110–126.
Trishchenko, A. P., Y. Luo, and K. V. Khlopenkov (2006), A method for downscaling MODIS land channels to 250-m spatial resolution using adaptive regression and normalization, *Proc. SPIE*, *6366*, doi:10.1117/12.689157.
Trnka, M., et al. (2010), Simple snow cover model for agrometeorological applications, *Agric. For. Meteorol.*, *150*, 1115–1127.
Vavrus, S. (2007), The role of terrestrial snow cover in the climate system, *Clim. Dyn.*, *29*, 73–88, doi:10.1007/s00382-007-0226-0.
Viterbo, P., and A. K. Betts (1999), The impact on ECMWF forecasts of changes to the albedo of the boreal forests in the presence of snow, *J. Geophys. Res.*, *104*, 27,803–27,810.
Wagner, J. A. (1973), The influence of average snow depth on monthly mean temperature anomaly, *Mon. Weather Rev.*, *101*, 624–626, doi:10.1175/1520-0493(1973)101<0624:TIOASD>2.3.CO;2.
Walsh, J. E., and B. Ross (1988), Sensitivity of 30-day dynamical forecasts to continental snow cover, *J. Clim.*, *1*, 739–754, doi:10.1175/1520-0442(1988)001<0739:SODDFT>2.0.CO;2.
Wang, Z., and X. Zeng (2010), Evaluation of snow albedo in land models for weather and climate studies, *J. Appl. Meteorol. Climatol.*, *49*, 363–380.
Xu, L., and P. A. Dirmeyer (2013), Snow–atmosphere coupling strength Part I: Effect of model biases, *J. Hydrometeorol.*, *14*, 389–403.
Zhang, Y., S. Wang, A. G. Barr, and T. A. Black (2008), Impact of snow cover on soil temperature and its simulation in a boreal aspen forest, *Cold Reg. Sci. Technol.*, *52*, 355–370.